1-1-2017

Atomic-Scale CoOx Species in Metal-Organic Frameworks for Oxygen Evolution Reaction

Shuo Dou
Hunan University

Chung-Li Dong
Tamkang University

Zhe Hu
University of Wollongong, zh865@uowmail.edu.au

Jeng-Lung Chen
Tamkang University

Yu-Cheng Huang
Tamkang University

See next page for additional authors

Atomic-Scale CoOx Species in Metal-Organic Frameworks for Oxygen Evolution Reaction

Abstract

The activity of electrocatalysts strongly depends on the number of active sites, which can be increased by downsizing electrocatalysts. Single-atom catalysts have attracted special attention due to atomic-scale active sites. However, it is a huge challenge to obtain atomic-scale CoO x catalysts. The Co-based metal-organic frameworks (MOFs) own atomically dispersed Co ions, which motivates to design a possible pathway to partially on-site transform these Co ions to active atomic-scale CoO x species, while reserving the highly porous features of MOFs. In this work, for the first time, the targeted on-site formation of atomic-scale CoO x species is realized in ZIF-67 by O 2 plasma. The abundant pores in ZIF-67 provide channels for O 2 plasma to activate the Co ions in MOFs to on-site produce atomic-scale CoO x species, which act as the active sites to catalyze the oxygen evolution reaction with an even better activity than RuO 2 .

Disciplines

Engineering | Physical Sciences and Mathematics

Publication Details

Dou, S., Dong, C., Hu, Z., Chen, J., Huang, Y., Tao, L., Yan, D., Chen, D., Shen, S., Chou, S. & Wang, S. (2017). Atomic-Scale CoOx Species in Metal-Organic Frameworks for Oxygen Evolution Reaction. Advanced Functional Materials, 27 (36), 1702546-1-1702546-8.

Authors

Shuo Dou, Chung-Li Dong, Zhe Hu, Jeng-Lung Chen, Yu-Cheng Huang, Li Tao, Dafeng Yan, Dawei Chen, Shaohua Shen, Shulei Chou, and Shuangyin Wang

Targeted On-site Formation of Atomic-scale CoO_x Species in Metal-Organic-Frameworks for Oxygen Evolution Reaction

Shuo Dou,[+],[a] Chung-Li Dong, [+],[b] Zhe Hu,[+],[c] Yu-Cheng Huang, [b] Jeng-lung Chen,[b] Li Tao,[a] Dafeng Yan,[a] Dawei Chen,[a] Jia Huo,[a] Shaohua Shen,[d,*] Shulei Chou,[c,*] Bo Wang, [e] and Shuangyin Wang [a,*]

[a] State Key Laboratory of Chem/Bio-Sensing and Chemometrics, College of Chemistry and Chemical Engineering, Hunan University, Changsha, 410082, P. R.China.
E-mail: shuangyinwang@hnu.edu.cn

[b] Department of Physics, Tamkang University, Tamsui, Taiwan.

[c] Institute for Superconducting and Electronic Materials, University of Wollongong, Wollongong, New South Wales 2522, Australia.

[d] State Key Laboratory of Multiphase Flow in Power Engineering, Xi'an Jiaotong University, Shaanxi 710049, P. R. China.

[e] School of Chemistry, Beijing Institute of Technology, South Zhongguancun Street, Beijing, 10081, P. R. China.Address line 1, Address line 2, postcode, Country

[+]These authors contributed equally to this work

Abstract:

The activity of electrocatalysts strongly depends on the number of active sites, which can be increased by down-sizing electrocatalysts. Single-atom catalysts have attracted special attentions due to the atomic-scale active sites. However, it is a huge challenge to obtain atomic-scale CoO_x catalysts. While, the Co-based metal-organic-frameworks (MOFs) own atomically-dispersed Co ions, which motivates us to design a possible pathway to partially on-site transform these Co ions to active atomic-scale CoO_x species while reserving the highly-porous features of MOFs. In this work, we, for the first time, realized the targeted on-site formation of atomic-scale CoO_x species in ZIF-67 by O_2 plasma. The abundant pores in ZIF-67 provide channels for O_2 plasma to activate the Co ions in MOFs to on-site produce atomic-scale CoO_x species, which act as the active sites to catalyze the oxygen evolution reaction with an even better activity than RuO_2.

Keywords: electrocatalyst, oxygen evolution, metal-organic frameworks, atomic-scale CoO_x

1. Introduction

The electrochemical oxygen evolution reaction (OER) has been regarded as the core process in metal-air batteries and water splitting devices.[1-2] Due to the sluggish reaction kinetics, exploring highly efficient OER electrocatalysts is of significant demand. Noble metal oxides of Ru/Ir are the most active OER electrocatalysts for the low overpotential and large current density.[3] However, they are suffered from high cost and poor durability, which hinders the application of these materials.

To solve this problem, many studies have been carried out to develop highly efficient and low-cost OER electrocatalysts, such as developing transition metal compound and even metal-free materials[4]. Cobalt-based materials [5-7] are promising alternatives to replace noble metal oxides for OER. Especially, Co oxides have been extensively developed due to their high performance.[8-12] Since the electrocatalytic process only occurs on the surface of catalysts, it is essential to downsize Co-based species with more catalytically active sites exposed. To this end, pushing the size limit of catalyts to the atom level is a promising strategy.[13] For this purpose, we turn our attention onto metal organic frameworks (MOFs), in which metal centers are atomically distributed. Specifically, in ZIF-67, a Co-based MOF, Co^{2+} are uniformly distributed at the atomic scale. The question is how to make use of these Co species as active sites for OER. Previously, studies on MOFs directively used as OER electrocatlaysts have been roported.[14-15] But intrinsically, ZIF-67 shows poor catalytic activity for OER. The challenge is how to on-site transform the atomically distributed Co^{2+} in MOFs into atomic-scale active sites for OER. Co-based electrocatalysts derived from MOFs by direct carbonization have been widely reported.[16-18] The sever structural shrinkage during carbonization usually leads to a huge decrease of the surface area of MOFs precursors. In addition, most of these Co-based electrocatalysts exist in the form of nanoparticles with limited active sites exposed. Therefore, it is essential to develop a strategy to obtain atomic-

scale CoO_x species with every active species exposed to catalyze OER while reserving the abundant pores in MOFs to facilitate the mass transport of incoming reactants and outgoing products.

O_2 plasma is a powerful tool to modify materials for its etching effect, and the metal atom exposed in the O_2 atmosphere would be inevitable oxidized. Fortunately, the formation of Co oxide species are beneficial for electrocatalyzing OER. Thus, in this work, we have applied O_2 plasma to treat ZIF-67 to on-site produce atomic-scale CoO_x species in ZIFs (CoO_x-ZIF) as an efficient OER electrocatalyst. The porous structure of MOFs provides pathways for O_2 plasma to activate the atomically dispersed Co species. In addition, plasma is highly efficient for a rapid treatment, which would not severely destroy the bulk structure of MOFs during the treatment. The O_2 plasma treatment on ZIF-67 leads to the on-site formation of atomic-scale CoO_x species in MOFs with high surface area. The as-obtained CoO_x species in ZIF-67 show advanced electrocatalytic performance for OER. Coupling the CoO_x-ZIF with conductive supports led to even better activity than RuO_2.

2. Experimental Section

2.1 Materials preparation

The ZIF-67 was synthesized according to a literature.[19] In brief, 1.455 g cobalt nitrate hexahydrate ($Co(NO_3)_2$•$6H_2O$) was dissolved in 80 mL methanol. Another solution with 80 mL methanol and 1.642 g 2-methylimidazole (MeIM) was slowly added to the above $Co(NO_3)_2$ solution under stirring for 30 s. The whole mixture was kept at room temperature for 24 h silently. ZIF-67 was obtained by centrifugation and washing with methanol for 5 times and dried at 60°C in a vacuum oven. For the O_2 plasma treatment, we applied the RF power of 200 W, and the pressure was controlled at 120 Pa, and the treating time was 1 h. Different treating times were also conducted to optimize the OER performance. For the reference sample, pure ZIF-67 was placed in a tube furnace and annealed at 800 °C under N_2

with a heating rate of 5 °C min^{-1} for 2 hours, and after the tube furnace cooled to room temperature, pyrolyzed ZIF-67 was obtained.

2.2 Physical characterization

Scanning electron microscope (SEM, Hitachi, S-4800) and transmission electron microscope (TEM, FEI, Tecnai G2 F20) were used to observe the morphology of CoO_x-ZIF. Atomic resolution analytical microscope (ARM) investigations were performed using a 200 kV JEOL 2011 instrument. The X-ray diffraction (XRD) measurements used a Rigaku D/MAX 2500 diffractometer with Cu Kα radiation. X-ray photoelectron spectroscopic (XPS) measurements were carried out on an AXIS ULTRA (Kratos Analytical). The Brunauer-Emmmett-Teller (BET) specific surface area characterizations of the samples were detected by a nitrogen adsorption-desorption method (SSA-4200). The synchrotron x-ray absorption spectroscopy Co K-edge was carried out at BL17C at the National Synchrotron Radiation Research Center, Taiwan.

2.3 Electrochemical measurement

4 mg of CoO_x-ZIF was dispersed in 2 mL ethanol followed by ultrasonication for 30 min, 100 μL 5 % Nafion solution was added to the dispersion and ultrasonication for another 30 min to obtain the catalytic ink. The electrochemical measurements were performed in a three electrodes system using an electrochemical work station (CHI 760E) with Pt mesh as counter electrode and saturated calomel electrode (SCE) as reference electrode. The working electrode for OER testing was prepared by dripping 20 μL catalytic ink on a glassy carbon (5 mm in diameter) and dried under air atmosphere. 1.0 M KOH aqueous solution was used as electrolyte. All of the potentials were calibrated to a reversible hydrogen electrode (RHE) according to the Nernst equation $E(\mathrm{RHE}) = E(\mathrm{SCE}) + 0.0591 \times \mathrm{pH} + 0.24$. The polarization curves in this study were all corrected by *iR*-compensation.

The mechanism of OER was studied by a rotating ring-disk electrode (RRDE-3, ALS). The testing method was according to the previously reports.[16, 20] Firstly, the content of the formed

HO_2^- was tested by fixing the ring potential at 1.5 V vs. RHE in O_2-saturated 1 M KOH solution and collecting the ring current at a scan rate of 2mV s^{-1} under a rotation rate of 1600 rpm. The Faradaic efficiency (ε) was determined by collecting the ring current when fixing the disk current at 200 μA and ring potential at 0.4 V vs. RHE in N_2-saturated 1 M KOH solution.

$$\varepsilon = \frac{I_r}{I_d * N}$$

Where I_d is the disk current, I_r is the ring current, and N is the current collection efficiency (0.21 in this study) which was determined by IrO_2 catalyst thin film electrode.

The electrochemical surface area (ECSA) was evaluated by measuring the double layer capacitance method via CVs at different scan rate from 20 to 100 mV s^{-1} in the range of no Faradaic processes occurred. The electrochemical double-layer capacitance was given according to the following equation [21]:

$$C_{dl} = \frac{I_c}{v}$$

Where C_{dl} is the double layer capacitance, I_c is the charging current, and v is the scan rate.

The ECSA could be calculated from the double layer capacitance according to:

$$ECSA = \frac{C_{dl}}{C_s}$$

Where C_s is the specific capacitance of the sample or the capacitance of an atomically smooth planar surface of the material per unit area under identical electrolyte conditions, and in this study, the C_s is 27 μF cm^{-2} according to the literature [21].

The turnover frequency (TOF) was evaluated by the following equation [15]:

$$TOF = \frac{J \times A}{4 \times m \times F}$$

Where, J is the current density at overpotential of 320 mV. A and m are the area of the electrode and the number of moles of the active materials that were deposited onto the electrode, respectively. F is the Faraday constant (96485 C mol^{-1}).

3. Results and Discussion

As illustrated in **Figure 1a**, O_2-plasma was applied to treat ZIF-67. In this way, atomic-scale CoO_x species are on-site formed in MOFs while reserving the porous structure of MOFs through the highly-efficient and mild partial oxidation by O_2 plasma. The surface morphology was first examined with SEM. It can be seen from **Figure 1b** that ZIF-67 shows a typical rhombic dodecahedral structure with a smooth surface.[22] After treatment by O_2 plasma for 1 h, lots of visible pores are present on the surface of ZIF-67, and the dodecahedral morphology is partially broken to fragments as shown in **Figure 1c**. From the optical observation of ZIF-67 and CoO_x-ZIF in **Figure S1a&b**, ZIF-67 displays a purple color. After O_2-plasma treatment, the color of the CoO_x-ZIF changes to dark purple, due to the change of absorbance. To investigate the crystalline structure change, the XRD measurement was carried out (**Figure 1d**). The patterns of ZIF-67 agree well with the simulative structure and the CoO_x-ZIF shows the similar pattern, which demonstrates that the main bulk structure of the as-treated sample is still ZIF-67. However, the diffraction intensity of CoO_x-ZIF is weakened, and careful comparation, it could be found that there is a little shift in the XRD pattern of CoO_x-ZIF relative to that of pure ZIF-67 presents in the **Figure 1d** and S2. These are mainly due to that the O_2 plasma destroyed the original crystal structure of ZIF-67, and defects are generated by the plasma etching as discussed in the literature.[23] Besides, no characteristic XRD peaks of crystalline CoO_x can be found in CoO_x-ZIF. The FT-IR spectrum was also used to observe the change of ligand before and after plasma treatment. As shown in Figure S3, the absorption band at 425 and 1580 cm^{-1} are assigned to the stretching vibration of Co-N and C=N, respectively. The bands at 1420 cm^{-1} are associated with the entire ring stretching and the bands in the region of 800~1350 cm^{-1} are for the in-plane bending of the ring while those below 800 cm^{-1} are related to the out-of-plane bending. The similar FT-IR spectra in Figure S3 also indicate that the main framework of CoOx-ZIF is still ZIF-67 structure after O_2 plasma treatment.

To study the chemical state of CoO_x-ZIF, X-ray photoelectron spectroscopic (XPS) measurements were carried out. It could be found from the survey spectra of ZIF-67 and CoO_x-ZIF (**Figure S4a**) that the atom ratio of N to Co is 4.72 in ZIF-67 and 3.46 in CoO_x-ZIF, indicating Co-N coordination bonds were partially destroyed by plasma. In ZIF-67, the Co 2p 3/2 peaks could be deconvoluted into two components: the Co-N_x peak at 781.2 eV and the satellite peaks.[24] After O_2 plasma treatment, the Co 2p 3/2 peak of CoO_x-ZIF shows a slight broadening and shifting to lower binding energy (**Figure S4b**). The Co 2p 3/2 peaks in CoO_x-ZIF could be further deconvoluted to another peak at 780.2 eV, which could be related to the formed CoO_x species (**Figure 1e**).[25] Similar to that of Co 2p 3/2, the O 1s of CoO_x-ZIF exhibits broadening and shifting to lower binding energy (**Figure S4c**), due to the formation of typical metal-oxygen bond[26]. These results confirm that Co-N coordination bonds in ZIF-67 were partially broken and the Co species was oxidized to form CoO_x species by O_2 plasma. According to the deconvoluted Co 2p 3/2, we could evaluate that the atomic percentage of oxidized Co is about 29.7% (**Figure 1e**). Besides, the O_2 plasma treatment on ZIF-67 also resulted in a slight oxidation of carbon species as evidenced by the increased C-O/O-C=O percentage (from 6.98% to 10.24%) in C 1s XPS peaks (**Figure S5**).

From the TEM images (**Figure 2a**) and high-angle annular dark-field scanning TEM (HAADF-STEM, **Figure 2b**), we could observe that the relatively rough surface was obtained on CoO_x-ZIF comparing to the smooth surface of ZIF-67 (**Figure S6**). No point- or ring-like patterns were observed in the selected area electron diffraction (SAED) pattern of CoO_x-ZIF in **Figure 2c**, indicating that no bulk particles of Co or Co oxides were formed by O_2 plasma. This was also demonstrated by the HRTEM in **Figure S7**, in which there was no lattice fringe of crystallized Co or Co oxides. From the element mapping of Co, O, C, N in **Figure 2d**, we could see that O element is also well dispersed in CoO_x-ZIF. Thus, the as-formed CoO_x species by O_2 plasma are of atomic-scale with excellent dispersion. We further used HAADF imaging in an aberration-corrected STEM to confirm that the obtained CoO_x species are

atomically dispersed. As shown in **Figure 2e** and **2f,** the heavier atom of Co (bright dots), which are partly marked by red circles, are well dispersed in the matrix with the size of about 0.2~0.3 nm, indicating Co is atomic-scale dispersed.

N_2 adsorption and desorption isotherm in **Figure S8** shows a typical microporous characteristic of ZIF-67 and CoO_x-ZIF. The CoO_x-ZIF displays a Brunauer-Emmett-Teller (BET) surface area of 1128.3 m^2g^{-1}, which is smaller than ZIF-67 (1690.9 m^2g^{-1}). The decrease of surface area after plasma treatment is because the plasma treatment partially destroyed the porous structure of ZIF-67 by the etching effect. However, the surface area is still relatively high for electrochemical applications. Besides, the plasma etching may generate mesopores, which would facilitate the electrolyte diffusion to active sites of electrocatalysts as confirmed by the pore distribution (**Figure S9**). Further more, as shown in **Figure S10**, the *g* value of CoO_x-ZIF in the electron paramagnetic resonance (EPR) decreases to 2.23 from 2.33 of pristine ZIF-67. The shift towards the value of 2.0023, the *g* value of free electron, indicates the CoO_x-ZIF displays higher conductivity.[27] Electron energy-loss spectroscopy (EELS) is a powerful technique for measuring the valences of Co.[28] **Figure S11** shows the EELS spectrum of CoO_x-ZIF and the area ratio of L_3/L_2 could be calculated to 2.69. The L_3/L_2 areal ratio of Co ion in the pure Co, CoO, and Co_3O_4 are 3.77, 2.9 and 2.43, respectively.[28] Compared with Co^{2+} in ZIF-67, the lower area ratio indicates that Co species was partially oxidized in CoO_x-ZIF. The redox behavior of the Co species could be evaluated by cyclic voltammetry (CV). As shown in **Figure S12**, redox peaks of Co 2+/3+ were present in both CoO_x-ZIF and ZIF-67, indicating both samples own Co^{2+}. Furthermore, a small redox peaks at around 1.4 V (equilibrium potentials of Co 3+/4+) could be found in CoO_x-ZIF but absent in ZIF-67, proving the partial oxidation of Co species in CoO_x-ZIF.[29]

To determine the fine structure and oxidation state of Co species in ZIF-67, X-ray absorption spectroscopy (XAS), including X-ray absorption near edge structure (XANES) and extend X-ray absorption fine structure (EXAFS) spectra were performed. **Figure 3a** presents

the Co K-edge XANES of ZIF-67 and CoO_x-ZIF. The Co K-edge is mainly originated from the electron transition from Co 1s to Co 4p unoccupied orbitals. After plasma treatment, the spectrum of CoO_x-ZIF is similar to CoO, suggesting formation of Co-O bond. The small prominent pre-edge feature around 7709 eV in ZIF-67 and CoO_x-ZIF is ascribed to the dipole forbidden transition from 1s to 3d states, and thus it can be normally regarded as the amount of unoccupied 3d states, and this further indicates that CoO_x-ZIF still remains the ZIF structure.[30] **Figure 3b** presents the overlaid spectra of ZIF-67 and CoO_x-ZIF. Notably, the intensity of this small feature is higher in ZIF-67 than CoO_x-ZIF which indicates the higher oxidized states of Co in ZIF-67 than in CoO_x-ZIF. However, this argument is contradictory to the result from shift of main absorption peak. The main absorption peak (indicated by the vertical bar) of CoO_x-ZIF in **Figure 3b** is enhanced, indicating CoO_x-ZIF loses some charges at Co site and thus increases the oxidation state, shifting the absorption peak as well as the absorption edge to higher energy. Consequently, the change of intensity of dipole forbidden small feature cannot be simply attributable to the 3d unoccupied states, but can be associated with the degree of symmetry of coordinated environment. Thus, the lower intensity observed in CoO_x-ZIF indicates more symmetrical atomic structures around Co after plasma treatment. Moreover, the rising absorption edge around 7715-7720 eV is attributed to the localized Co 1s to 4p excitation that is originated from interaction of charge transfer between ligand and metal. Therefore the decline of the intensity of rising absorption region may be due to the fact that there are less Co-N bond after modification. The suspended Co is ligated by oxygen after O_2-plasma process and would delocalize the orbital, leading to decrease the intensity. To further clarify the effect of modification on atomic structure around the Co atoms, the Fourier transfer (FT) of the EXAFS $k^3\chi$ at Co K-edge is displayed in **Figure 3c**. Inset of **Figure 3c** presents the $k^3\chi$ EXAFS oscillations for ZIF-67 and CoO_x-ZIF. The oscillation behavior is different between ZIF-67 and CoO_x-ZIF, and more complex oscillation is observed in CoO_x-ZIF, suggesting atomic structure undergoes modulation in CoO_x-ZIF. In the FT, the main peak

(marked by a star) is due to Co-N bond. The additional feature on the shoulder (marked by an arrow) is arisen from the formation of Co-O bond. The EXAFS demonstrates that the Co-O is formed in CoO_x-ZIF after modification and presence of oxygen in CoO_x-ZIF would lead to different charge distribution compared with ZIF-67 which is mainly consisted of Co-N bonds. Notably, the oxygen has electron negativity ~3.44 which is higher than nitrogen ~3.04. Thus, oxygen can attract electron from Co sites more significantly than nitrogen and therefore give rise to higher unoccupied orbitals at Co sites in CoO_x-ZIF (**Figure 3b**). This figure also includes the spectra of reference Co metal. As you can see the Co metal in **Figure 3a** is very different from ZIF-67, CoO_x-ZIF and Co-oxides. Also, the EXAFS in **Figure 3c** present the different oscillation (inset) and the FT spectra. All these results suggest the formation of Co-Co bond is unlikely in CoO_x-ZIF samples, which indicates the absence of metallic Co.

The electrocatalytic activity of the CoO_x-ZIF towards OER was studied in 1 M KOH with a mass loading of 0.2 mg cm^{-2}. Linear sweep voltammetry (LSV) curves of ZIF-67 and CoO_x-ZIF are shown in **Figure 4a**, from which we can see that the onset potential of OER on CoO_x-ZIF is smaller than that on ZIF-67. To accurately evaluate the activity, the potential at the current density of 10 mA cm^{-2} is usually used as an indicator. The ZIF-67 requires a potential of 1.63 V *vs*. RHE to reach the current density of 10 mA cm^{-2}. Notably, the potential at 10 mA cm^{-2} shifts to 1.548 V on CoO_x-ZIF, which is almost the same as RuO_2. The negatively shifted potential indicates the positive effect of O_2-plasma. In ZIF-67, Co species bond with N atoms from the MeIM ligand. The destructive effect of plasma etching leads to the break of the Co-N coordination bond and the suspended Co species was rapidly oxidized in the presence of O_2 to produce CoO_x. The existed CoO_x species enhances the OER performance of ZIF-67. It is well known that the poor conductivity of ZIF-67 hinders their electrocatalytic applications. Thus, we added conductive carbon to improve the conductivity of CoO_x-ZIF (CoO_x-ZIF/C). The CoO_x-ZIF/C exhibits even better performance than RuO_2 (**Figure 4a**). It is also necessary to compare the specific activity of CoO_x-ZIF with ZIF-67 (current per BET area). As shown

in **Figure 4b**, when comparing the specific activity at 1.6 V, the as-prepared CoO_x-ZIF shows a current of 0.0434 mA cm^{-2}_{BET}, which is 12 times higher than that of pristine ZIF-67 (0.0034 mA cm^{-2}_{BET}), proving the excellent intrinsic activity of the atomic-scale CoO_x. To identify the electrocatalytic active site is the formed CoO_x instead of carbon and nitrogen atoms in the ligand. We employed KSCN to poison the CoO_x by blocking Co sites[31]. As expectation, there is negligible OER current present in the LSV polarization curve in the Figure S13, indicating that the carbon and nitrogen atoms are not the real electrocatalytic active sites for OER.

The Tafel plots were also collected to investigate the OER kinetics in **Figure 4c**. The CoO_x-ZIF displays a smaller Tafel slope (70.3 mV dec^{-1}) than pristine ZIF-67 (108.8 mV dec^{-1}), which demonstrates the intrinsic reason for CoO_x-ZIF owning better OER activity than pristine ZIF-67. In addiation, the exchange current densities measure the catalytic activity of the films at overpotential of 0 V. The exchange current density of the as-prepared CoO_x-ZIF was calculated to be 3.02×10^{-7} A cm^{-2}, which is larger than most Co-based OER electrocatalysts in literarutes.[32-34] In alkaline condition, the mechanistic scheme of electrochemical water splitting could be descriped as [35-36]:

$$M+OH^- \rightarrow M\text{-}OH+e^- \quad (1)$$

$$M\text{-}OH+OH^- \rightarrow M\text{-}O^-+H_2O \quad (2)$$

$$M\text{-}O^- \rightarrow M\text{-}O+e^- \quad (3)$$

$$2M\text{-}O \rightarrow 2M+O_2 \quad (4)$$

M denotes the catalytic active site. According to the value of obtained Tafel slope of CoO_x-ZIF, it could be deduced that the first electron transfer step, associated with the adsorption of OH^-, is followed by a subsequent chemical step-the recombination of the surface OH species-involved in the rate determining step for the CoO_x-ZIF.[33]

The fitted electrochemical impedance spectroscopy (EIS) indicates that the ohm resistance of CoO_x-ZIF (6.31 Ω) is smaller than that of ZIF-67 (7.60 Ω), which is consistent with the EPR results, indicating the improved conductivity of CoO_x-ZIF. On the other hand, the semi-circular diameter of CoO_x-ZIF (20.9 Ω) is also smaller than that of ZIF-67 (28.6 Ω), confirming the better electrocatalytic activity with a faster charge transfer for OER (**Figure 4d** and **Figure S14**). The operational stability is also very important. For most of the MOFs materials, the stability in acid or alkaline electrolyte is a challenge for the possible degradation of unsupported 3D framework upon exposure to electrolytes.[2] Luckily in this study, the adopted ZIFs materials have been proved with exceptional chemical stability in aqueous alkaline solution[37]. We investigated the operational stability of CoO_x-ZIF by measuring the LSV curves before and after CVs for 2000 cycles. As shown in **Figure S15**, after cycling, there is only a little decay of the onset potential, displaying a reasonable stability. The XRD pattern detected after cycling in **Figure S16** also shows that the ZIFs structure is still remained. As shown in Figure S17, the double layer capacitances (C_{dl}) of the pure ZIF-67 and the CoO_x-ZIF were evaluated by CVs to be 3.04 and 1.47 mF, respectively. The higher C_{dl} of CoO_x-ZIF indicates that after O_2 plasma treatment, larger active surface areas than the pure ZIF-67 was obtained. The calculated electrochemical surface area (ESCA) of 112.59 cm^{-2} for CoO_x-ZIF and 61.25 cm^{-2} for ZIF-67 further confirms that the formed atom-scaled CoO_x species provides more active sites for the OER. According to the study from Tang's group, the turnover frequency (TOF) based on the amount of Co atoms of CoO_x-ZIF was calculated to be 0.082 s^{-1} at an overpotential of 320 mV, which is larger than the TOF of pure ZIF-67 (0.019 s^{-1}).

To study the reaction mechanism of OER, we used rotating ring-disk electrode (RRDE) and collected the ring current by fixing the ring potential at 1.5 V vs. RHE in 1 M KOH solution at 1600 rpm. It can be seen from **Figure 4e** that the collected ring current is about 8~10 μA which is much lower than the disk current, indicating that the hydrogen peroxide formation

was negligible. When the potential is higher than 1.5 V, the ring current decreased obviously which indicates fewer peroxide intermediates formed at the high potential region.[20] Furthermore, the Faradaic efficiency (ε) was obtained to determine whether the rapidly increased current density is mainly originating from water oxidation rather than from side reactions. The disk current was first fixed at 200 μA to generate O_2 from CoO_x-ZIF and the surrounding Pt ring electrode was fixed at an ORR potential of 0.4 V to reduce the sweeping across O_2. As shown in **Figure 4f**, a ring current of 38.6 μA was detected, and subsequently a high Faradaic efficiency of 92% could be obtained. This suggests that the detected oxidation current is mainly attributed to OER process.

It should be pointed out that the catalyst is sensitive to the plasma treatment time, as discussed in **Figure S18** and **S19**. To further investigate the effect of O_2-Plasma on the ZIF-67, longer treatment time was performed on the ZIF-67 sample. It can be seen from the XRD pattern that ZIFs structure is entirely destroyed, and Co_3O_4 is obtained after treated for 5h. This is another evidence that Co-O bond could form during the O_2 plasma process, and excessive treatment results in the complete conversion of Cobalt ion to Co_3O_4. It should also be noticed that, at the 2θ of ~22°, characteristic peak of carbon presences in the XRD pattern which reveals that longer treatment and higher plasma energy induces the organic ligand carbonization. Different treated time results in different OER performance. Comparing the pristine ZIF-67 with the sample of plasma treated for different time, we could see that after 0.5 h treatment, the OER performance is obviously enhanced. However, when the treatment reaches to 2h, the over treated sample shows poor performance comparing to the 1h (CoO_x-ZIF). When the treatment time is 3h or 5h, similar performance could be seen from the figure, indicating Co_3O_4 particles are obtained at these times. The presence of Co_3O_4 provides active sites to catalyze OER, thus shows better OER performance than the pristine. However, the sample treated for 1h (CoO_x-ZIF) is more favorable to catalyze the OER, as atomic-scale CoO_x provide more catalytic active sites. Moreover, O_2-plasma treated ZIF-67 shows better

OER performance than the pyrolyzed ZIF-67 and pure commerical Co_3O_4 (**Figure S20**), confirming the advantages of the atomic-scale CoO_x catalysts.

The applied RF power of plasma could affect the OER performance of O_2-plasma treated ZIF-67, thus, we used different power of 50, 100, 200 and 300 W to treat the ZIF-67. As we can see in **Figure S21**, as the power increases, the OER activity of the treated samples become higher, this is because that higher power results in more Co-N coordinate bond to be broken, and more CoO_x as OER catalytic active sites would be obtained. While the RF power reaches up to 300 W, poor OER performance obtained probably due to that the ZIF-67 was overtreated and the porous structure of ZIF-67 was broken down. We can also see from **Figure S22** that no matter how much RF power was applied, the visible pores could be seen from the treated ZIF-67, and higher power results in more pores from 50 W to 300 W.

4. Conclusion

In summary, we have successfully obtained the atomic-scale CoO_x species in the MOFs through a simple but efficient plasma treatment. The atomic-scale CoO_x species provide rich active sites for OER, demonstrating highly efficient electrocatalytic activity, which is even better than RuO_2. The unique atomic-scale dispersed structure of MOFs provides excellent precursors for the on-site formation of atomic-scale catalyst species for OER. The abundant pores in the ZIF-67 provide channels for O_2 plasma to activate the atomic Co ions in MOFs to on-site produce atomic-scale CoO_x species. During the plasma treatment, the Co-N coordination bonds in the ZIFs were partially broken and the suspended Co species could be easily reacted with O_2 present in the system to obtain CoO_x species locally. The formed atomic-scale CoO_x species act as the active sites to catalyze the OER. Furthermore, the remained large surface area and etched surface of ZIFs ensures excellent mass transport during OER. This is the first work to directly activate MOFs by on-site forming atom-scale active species for electrocatalysis.

Acknowledgements

The authors acknowledge support from the National Natural Science Foundation of China (51402100 and 21573066), and the Provincial Natural Science Foundation of Hunan (2016JJ1006 and 2016TP1009).

References

[1] Jin S.,May K. J.,Gasteiger H. A.,Goodenough J. B., and Yang S. H., *Science,* 2011, **334**: 1383-1385.
[2] Mahmood A.,Guo W.,Tabassum H., and Zou R., *Adv. Energy. Mater.,* 2016, **6**: 1600423.
[3] McCrory C. C. L.,Jung S.,Peters J. C., and Jaramillo T. F., *J. Am. Chem. Soc.,* 2013, **135**: 16977-16987.
[4] Ong W. J.,Tan L. L.,Ng Y. H.,Yong S. T., and Chai S. P., *Chem. Rev.,* 2016, **116**: 7159.
[5] Wu L.,Li Q.,Wu C. H.,Zhu H.,Mendozagarcia A.,Shen B.,Guo J., and Sun S., *J. Am. Chem. Soc.,* 2015, **137**: 7071-7074.
[6] Surendranath Y.,Kanan M. W., and Nocera D. G., *J. Am. Chem. Soc.,* 2010, **132**: 16501-16509.
[7] Dou S.,Tao L.,Huo J.,Wang S., and Dai L., *Energy & Environmental Science,* 2016, **9**: 1320-1326.
[8] Wang H. Y.,Hung S. F.,Chen H. Y.,Chan T. S.,Chen H. M., and Liu B., *J. Am. Chem. Soc.,* 2016, **138**: 36-39.
[9] Xia W.,Zou R.,An L.,Xia D., and Guo S., *Energy & Environmental Science,* 2015, **8**: 568-576.
[10] Xu L.,Wang Z.,Wang J.,Xiao Z.,Huang X.,Liu Z., and Wang S., *Nanotechnology,* 2017, **28**: 165402.
[11] Dong D.,Liu Y., and Li J., *Part. Part. Syst. Char. ,* 2016, **33**: 887-895.
[12] Islam M. M.,Faisal S. N.,Akhter T.,Roy A. K.,Minett A. I.,Konstantinov K., and Shi X. D., *Part. Part. Syst. Char. ,* 2017: DOI: 10.1002/ppsc.201600386.
[13] Qiao B.,Wang A.,Yang X.,Allard L. F.,Jiang Z.,Cui Y.,Liu J.,Li J., and Zhang T., *Nat. Chem.,* 2011, **3**: 634-641.
[14] Lu X. F.,Liao P. Q.,Wang J. W.,Wu J. X.,Chen X. W.,He C. T.,Zhang J. P.,Li G. R., and Chen X. M., *J. Am. Chem. Soc.,* 2016, **138**: 8336.
[15] Zhao S.,Wang Y.,Dong J.,He C.-T.,Yin H.,An P.,Zhao K.,Zhang X.,Gao C., and Zhang L., *Nature Energy,* 2016, **1**: 16184.
[16] Ma T. Y.,Dai S.,Jaroniec M., and Qiao S. Z., *J. Am. Chem. Soc.,* 2014, **136**: 13925-13931.
[17] Yin P.,Yao T.,Wu Y.,Zheng L.,Lin Y.,Liu W.,Ju H.,Zhu J.,Hong X.,Deng Z.,Zhou G.,Wei S., and Li Y., *Angew. Chem. Int. Ed. Engl.,* 2016, **55**: 10800-10805.
[18] Xia B. Y.,Yan Y.,Li N.,Wu H. B.,Lou X. W., and Wang X., *Nature Energy,* 2016, **1**: 15006.
[19] Hou Y.,Li J.,Wen Z.,Cui S.,Yuan C., and Chen J., *Nano Energy,* 2015, **12**: 1-8.
[20] Chen P.,Xu K.,Zhou T.,Tong Y.,Wu J.,Cheng H.,Lu X.,Ding H.,Wu C., and Xie Y., *Angew. Chem. Int. Ed. Engl.,* 2016, **55**: 2488-2492.
[21] Mccrory C. C.,Jung S.,Peters J. C., and Jaramillo T. F., *J. Am. Chem. Soc.,* 2013, **135**: 16977-87.
[22] Meng F.,Zhong H.,Di B.,Yan J., and Zhang X., *J. Am. Chem. Soc.,* 2016, **138**: 10226-10231.
[23] Chen B.,Ockwig N. W.,Millward A. R.,Contreras D. S., and Yaghi O. M., *Angew. Chem. Int. Ed. Engl.,* 2005, **44**: 4745-4749.

[24] Artyushkova K.,Levendosky S.,Atanassov P., and Fulghum J., *Top. Catal.,* 2007, **46**: 263-275.
[25] Niu K.,Yang B.,Cui J.,Jin J.,Fu X.,Zhao Q., and Zhang J., *J. Power Sources,* 2013, **243**: 65-71.
[26] Zhang N.,Li X.,Ye H.,Chen S.,Ju H.,Liu D.,Lin Y.,Ye W.,Wang C., and Xu Q., *J. Am. Chem. Soc.,* 2016, **138**: 8928-8935.
[27] Fleker O.,Borenstein A.,Lavi R.,Benisvy L.,Ruthstein S., and Aurbach D., *Langmuir,* 2016, **32**: 4935-4944.
[28] Yuhas B. D.,Zitoun D. O.,Pauzauskie P. J.,He R., and Yang P., *Angew. Chem. Int. Ed. Engl.,* 2006, **45**: 420-423.
[29] Han B.,Qian D.,Risch M.,Chen H.,Chi M.,Meng Y. S., and Yang S. H., *J. Phy. Chem. Lett.,* 2015, **6**: 1357-1362.
[30] Pattengale B.,Yang S.,Ludwig J.,Huang Z.,Zhang X., and Huang J., *J. Am. Chem. Soc.,* 2016, **138**: 8072-8075.
[31] Yang C.,Fu L.,Zhu R., and Liu Z., *Phys. Chem. Chem. Phys.,* 2016, **18**: 4635-4642.
[32] Koza J. A.,He Z.,Miller A. S., and Switzer J. A., *Chem. Mater.,* 2012, **24**: 3567-3573.
[33] Liu Y. C.,Koza J. A., and Switzer J. A., Electrochim. Acta, 2014, **140**: 359-365.
[34] Zhang Y.,Xiao Q.,Guo X.,Zhang X.,Xue Y.,Lin J.,Xue Z.,Yan Y. M., and Sun K., *J. Power Sources,* 2015, **278**: 464-472.
[35] Dau H.,Limberg C.,Reier T.,Risch M.,Roggan S., and Strasser P., *ChemCatChem,* 2010, **2**: 724-761.
[36] Bockris J. O. M., *J. Electrochem. Soc.,* 1984, **131**: 290-302.
[37] Park K. S.,Ni Z.,Côté A. P.,Choi J. Y.,Huang R.,Uribe-Romo F. J.,Chae H. K.,O'Keeffe M., and Yaghi O. M., *Proc. Natl. Acad. Sci. U. S. A.,* 2006, **103**: 10186-10191.

Caption to figures

1. **Figure 1.** (a) Preparation of CoO_x-ZIF; SEM images of (b) pure ZIF-67 and (c) CoO_x-ZIF (the inset shows the enlarged images and the scale bar is 200 nm), (d) XRD patterns and (e) Co 2p 3/2 XPS peaks of ZIF-67 and CoO_x-ZIF.

2. **Figure 2.** (a) TEM and (b) HAADF-STEM images of CoO_x-ZIF and (c) the corresponding SAED pattern; (d) element mapping of Co, O, C, N in CoO_x-ZIF;(e), (f) enlarged HAADF-STEM images of CoO_x-ZIF (the atom of Co are marked by red circles).

3. **Figure 3.** (a) The XANES spectra at Co K-edge of ZIF-67, CoO_x-ZIF, and references: Co metal, CoO, and Co_3O_4; (b) The overlaid XANES spectra of ZIF-67 and CoO_x-ZIF; (c) The Fourier transfer spectra of at Co K-edge and (inset) $k^3\chi$ EXAFS oscillations for ZIF-67 and CoO_x-ZIF.

4. **Figure 4.** (a) LSV curves for OER on ZIF-67, CoO_x-ZIF, CoO_x-ZIF/C, and RuO_2; (b) normalized LSV curves on CoO_x-ZIF and ZIF-67 by BET surface area; (c) the corresponding Tafel plots from LSV curves; (d) EIS of CoO_x-ZIF and ZIF-67 recorded at a constant potential of 1.55 V vs. RHE; (e) Ring current of CoO_x-ZIF on an RRDE with a ring potential of 1.5 V in O_2-saturated 1 M KOH; (f) Ring current of CoO_x-ZIF on an RRDE with a ring potential of 0.40 V in N_2-saturated 1 M KOH.

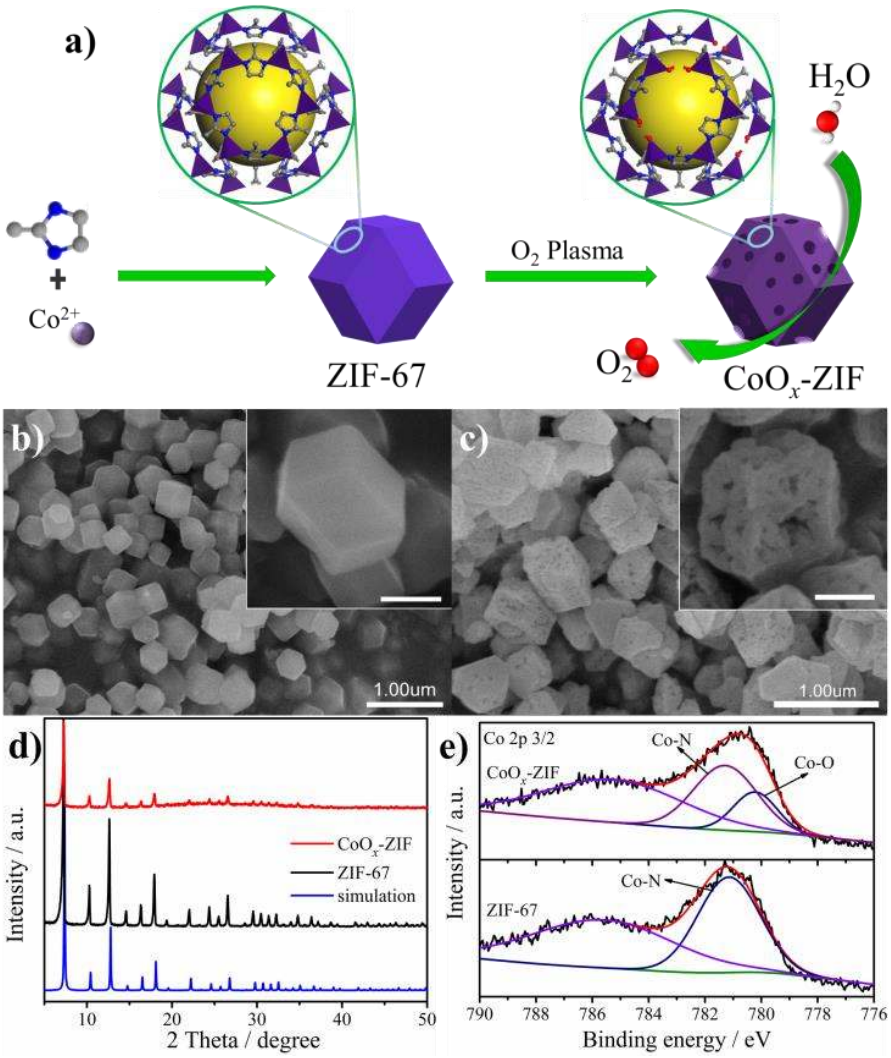

Figure 1. (a) Preparation of CoO_x-ZIF; SEM images of (b) pure ZIF-67 and (c) CoO_x-ZIF (the inset shows the enlarged images and the scale bar is 200 nm), (d) XRD patterns and (e) Co 2p 3/2 XPS peaks of ZIF-67 and CoO_x-ZIF.

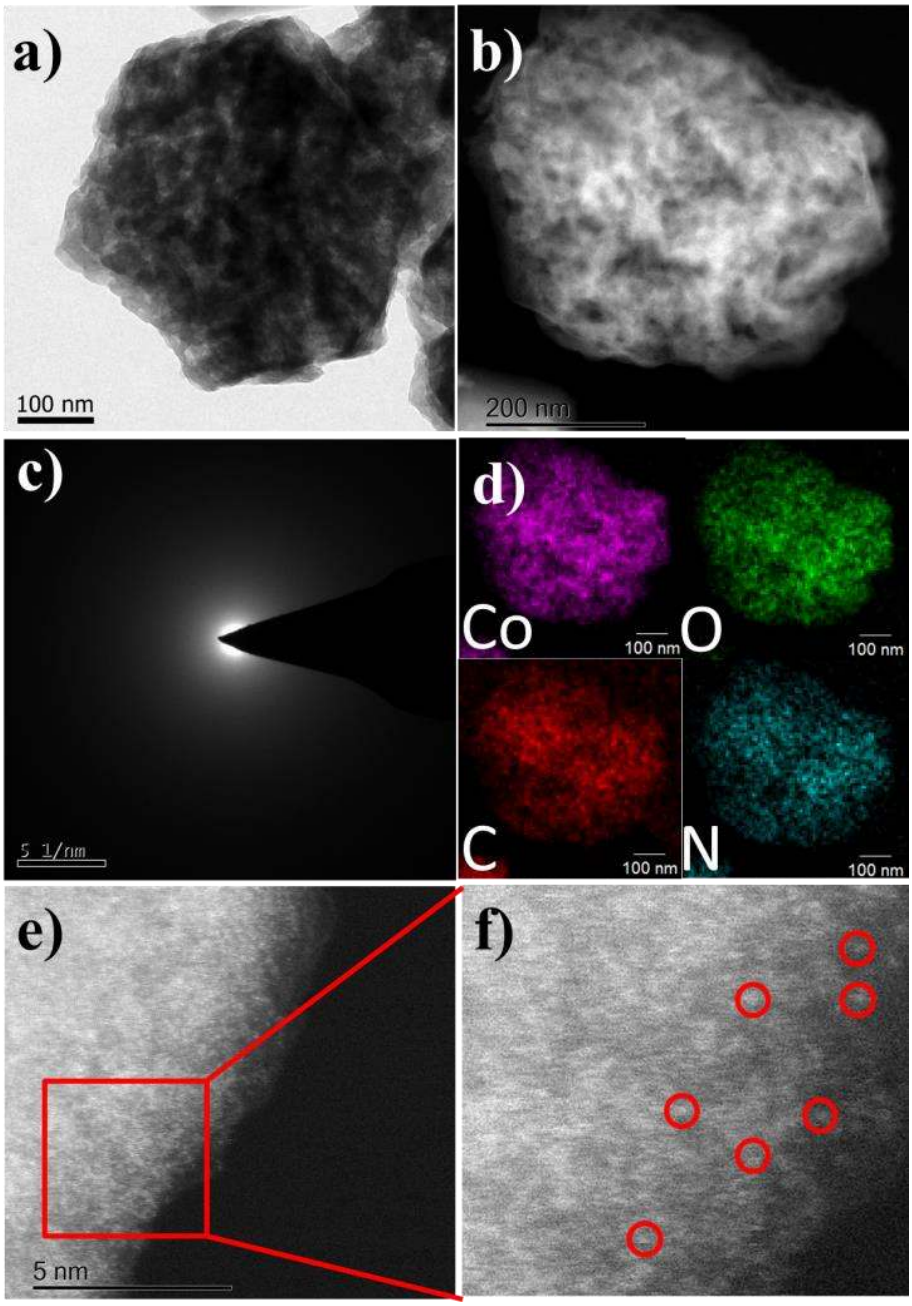

Figure 2. (a) TEM and (b) HAADF-STEM images of CoO_x-ZIF and (c) the corresponding SAED pattern; (d) element mapping of Co, O, C, N in CoO_x-ZIF;(e), (f) enlarged HAADF-STEM images of CoO_x-ZIF (the atom of Co are marked by red circles).

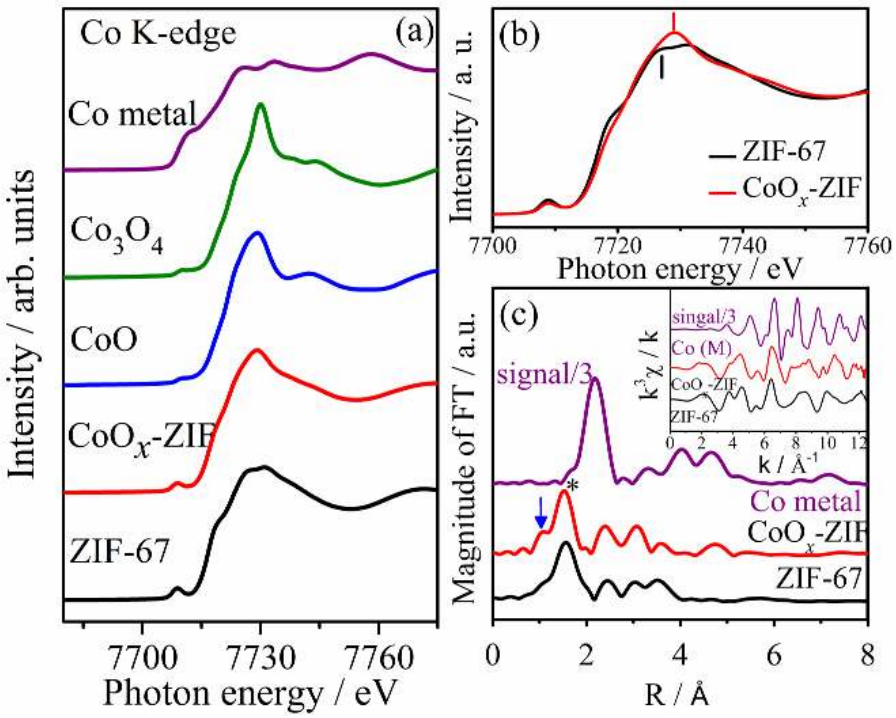

Figure 3. (a) The XANES spectra at Co K-edge of ZIF-67, CoO_x-ZIF, and references: Co metal, CoO, and Co_3O_4; (b) The overlaid XANES spectra of ZIF-67 and CoO_x-ZIF; (c) The Fourier transfer spectra of at Co K-edge and (inset) $k^3\chi$ EXAFS oscillations for ZIF-67 and CoO_x-ZIF.

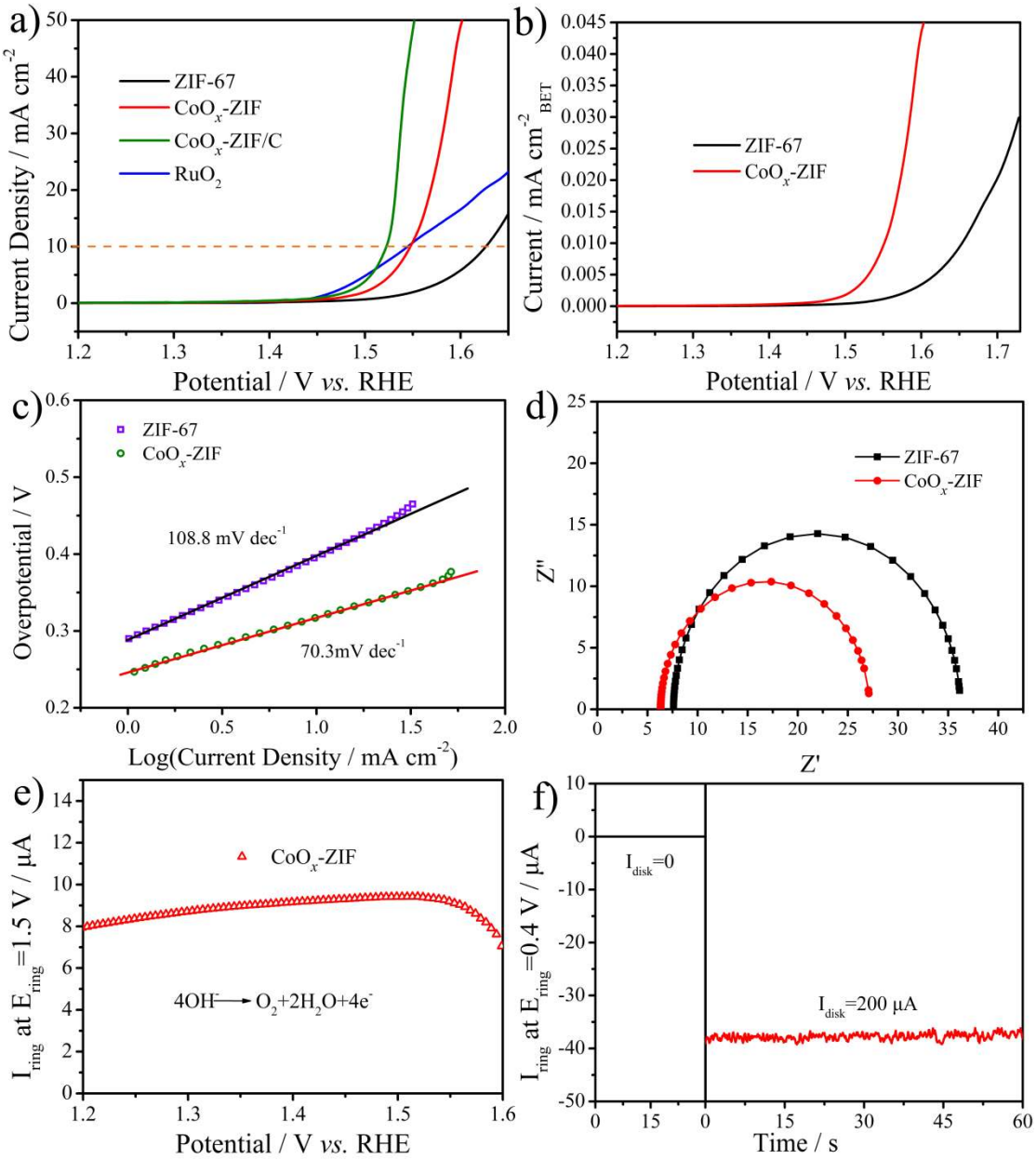

Figure 4. (a) LSV curves for OER on ZIF-67, CoO_x-ZIF, CoO_x-ZIF/C, and RuO_2; (b) normalized LSV curves on CoO_x-ZIF and ZIF-67 by BET surface area; (c) the corresponding Tafel plots from LSV curves; (d) EIS of CoO_x-ZIF and ZIF-67 recorded at a constant potential of 1.55 V vs. RHE; (e) Ring current of CoO_x-ZIF on an RRDE with a ring potential of 1.5 V in O_2-saturated 1 M KOH; (f) Ring current of CoO_x-ZIF on an RRDE with a ring potential of 0.40 V in N_2-saturated 1 M KOH.

Supporting Information

Targeted On-site Formation of Atomic-scale CoO_x Species in Metal-Organic-Frameworks for Oxygen Evolution Reaction

Shuo Dou,[+],[a] Chung-Li Dong, [+],[b] Zhe Hu,[+],[c] Yu-Cheng Huang, [b] Jeng-lung Chen,[b] Li Tao,[a] Dafeng Yan,[a] Dawei Chen,[a] Jia Huo,[a] Shaohua Shen,[d,*] Shulei Chou,[c,*] Bo Wang, [e] and Shuangyin Wang [a,*]

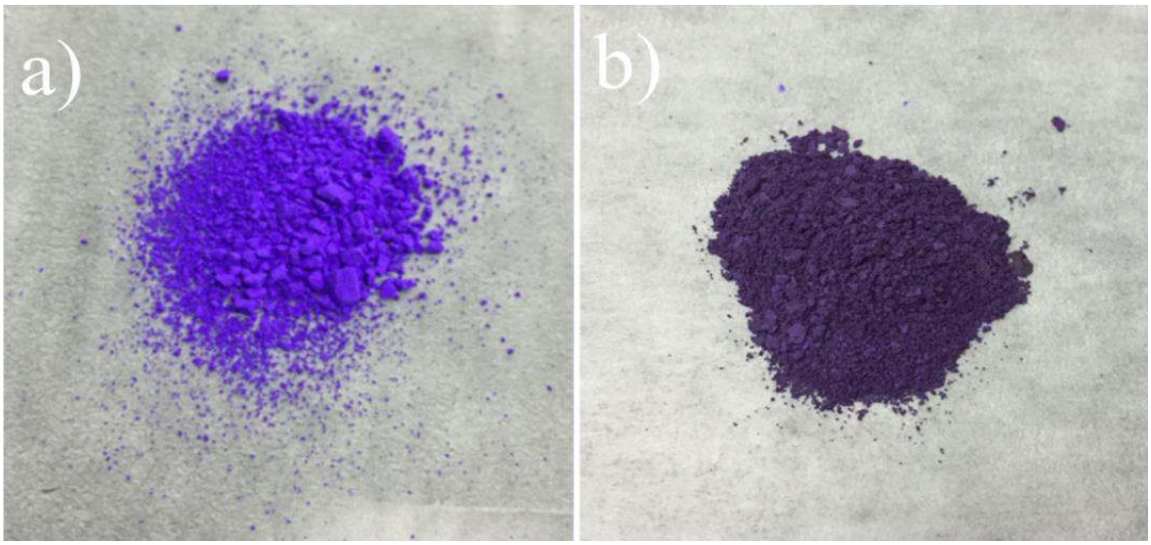

Figure S1. **The optical images of pure ZIF-67(a) and CoO_x-ZIF(b).**

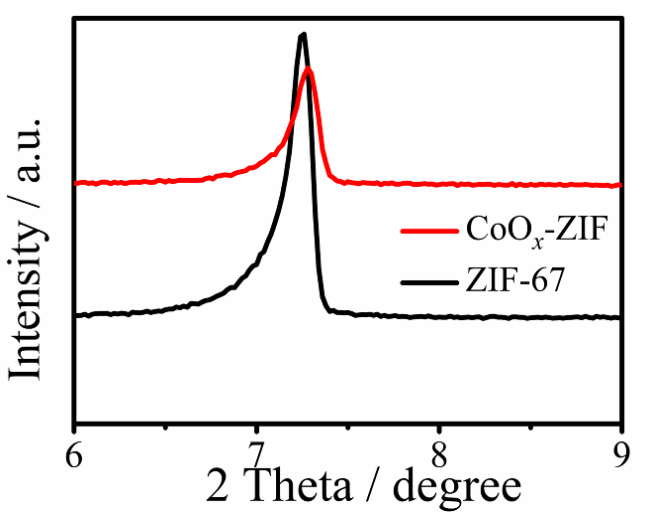

Figure S2. **The amplifying comparison of XRD patterns on pure ZIF-67 and CoO$_x$-ZIF.**

Table S1. **XRD parameters of pure ZIF-67 and CoO$_x$-ZIF.**

	CoO$_x$-ZIF	ZIF-67
	2-Theta (degree)	2-Theta (degree)
1	7.28	7.257
2	10.299	10.282
3	12.64	12.621
4	14.62	14.6
5	16.377	16.323
6	17.93	17.92
7	19.418	19.38
8	22.016	22.038
9	24.404	24.38
10	25.559	25.499
11	26.561	26.559
12	29.578	29.539
13	30.504	30.462
14	31.413	31.362
15	32.341	32.261
16	33.728	33.151
17	34.02	33.996
18	34.817	34.8
19	36.442	36.398
20	37.171	37.18
21	38.754	38.697

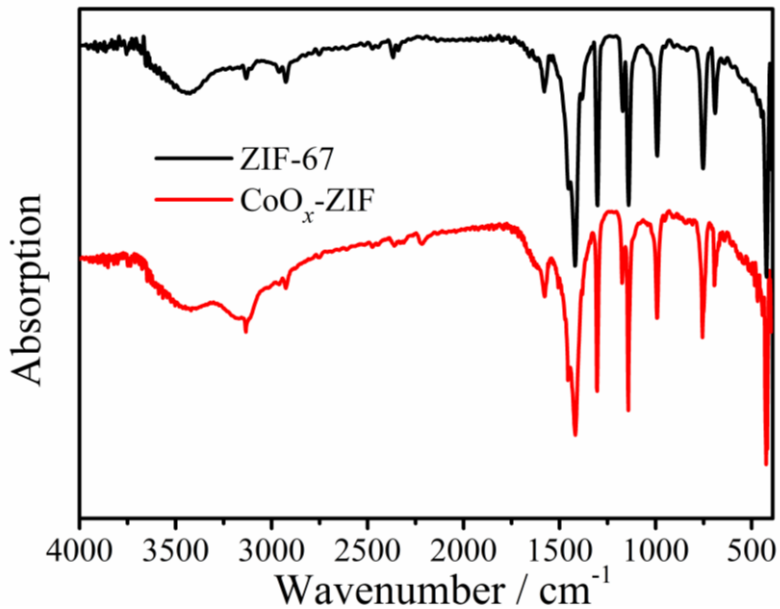

Figure S3. **FTIR spectrum of ZIF-67and CoO_x-ZIF.**

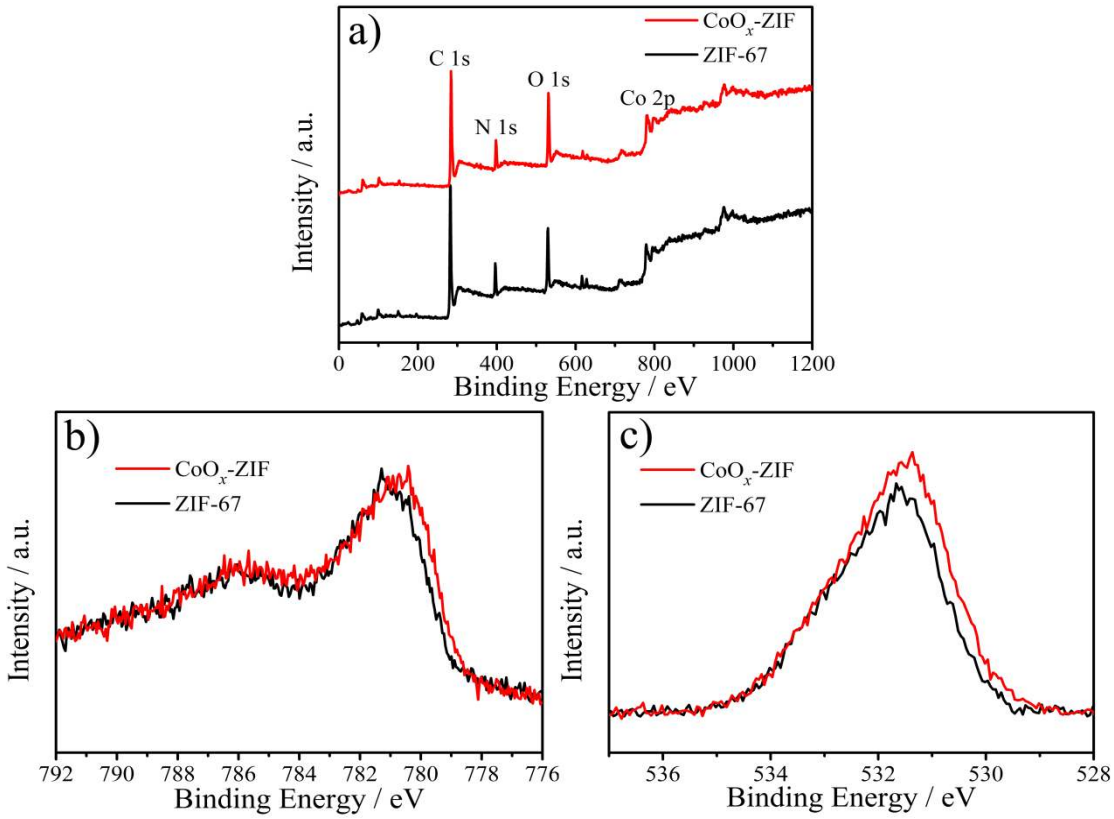

Figure S4. **(a) XPS survey spectra of ZIF-67and CoO$_x$-ZIF; (b) Co 2p2/3 XPS peaks of ZIF-67and CoO$_x$-ZIF; (c) O 1s XPS peaks of ZIF-67and CoO$_x$-ZIF.**

Table S2. **Summarization the content of different elements in ZIF-67and CoO$_x$-ZIF**

Sample	C (At%)	N (At%)	O (At%)	Co (At%)
ZIF-67	71.91	8.34	17.34	2.41
CoO$_x$-ZIF	75.38	8.78	13.98	1.86

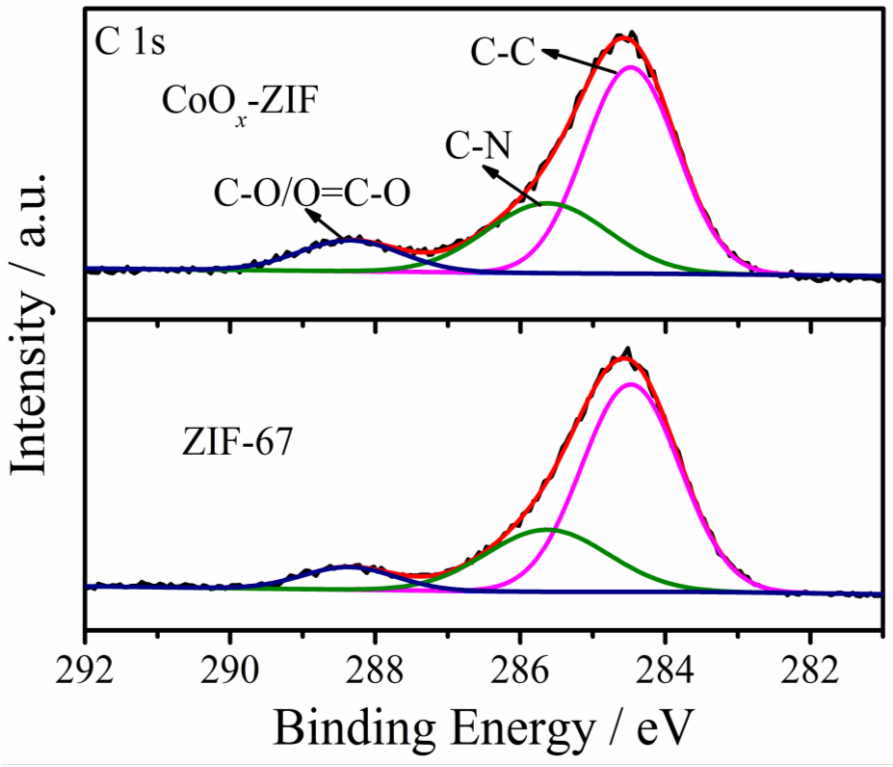

Figure S5. **C 1s XPS peaks of ZIF-67and CoO$_x$-ZIF.**

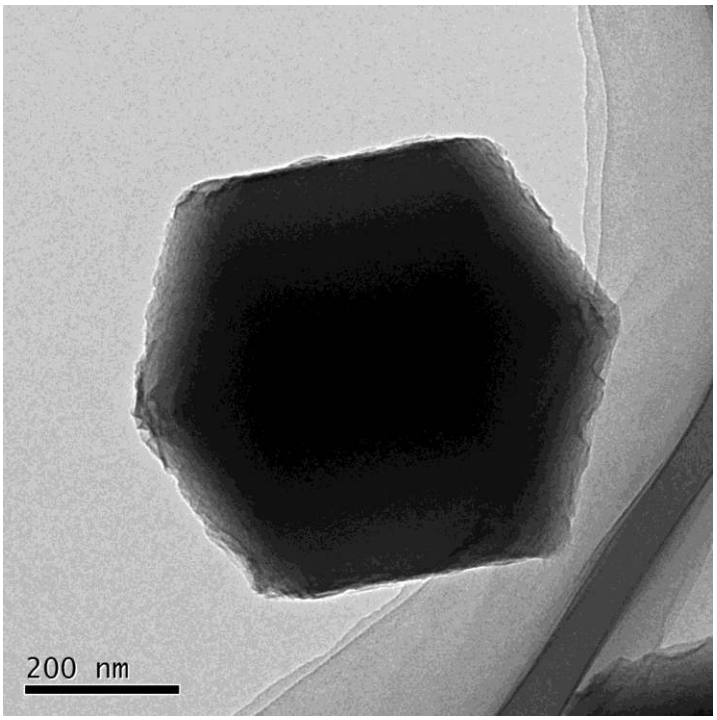

Figure S6. **TEM image of pristine ZIF-67.**

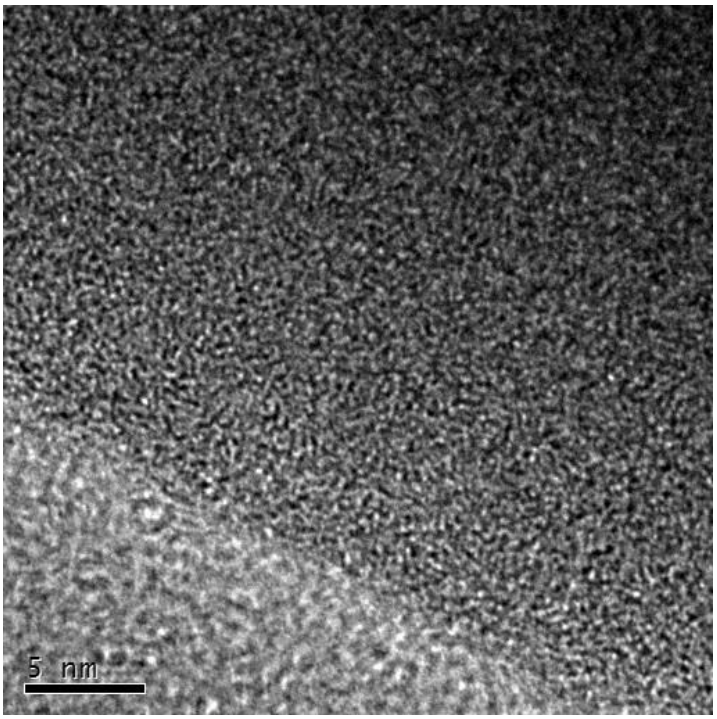

Figure S7. **HRTEM image of CoO_x-ZIF.**

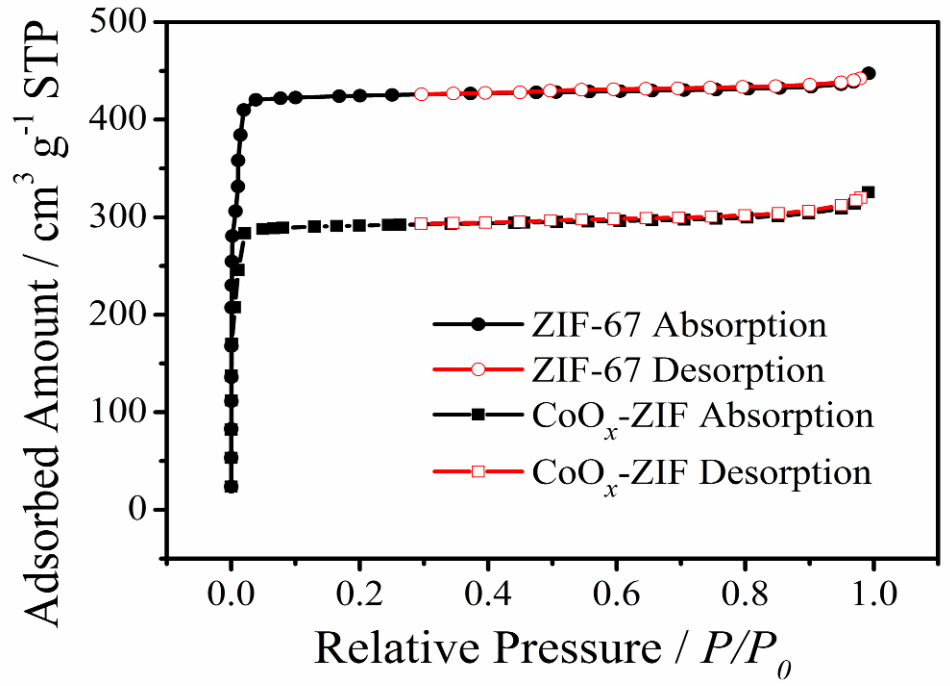

Figure S8. **Nitrogen sorption isotherms of ZIF-67 and CoO_x-ZIF.**

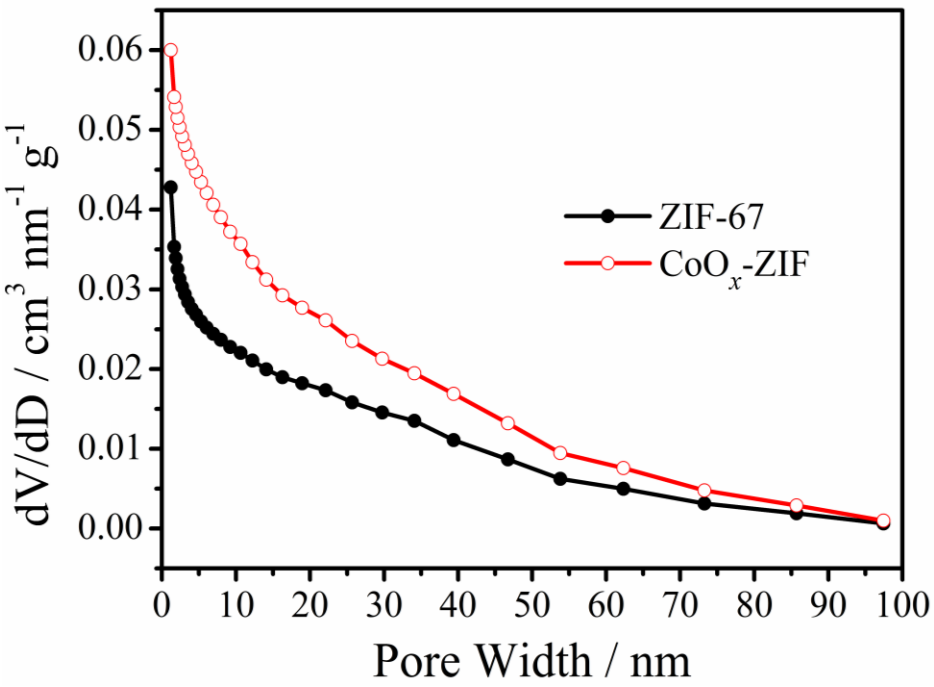

Figure S9. **Pore size distribution of ZIF-67and CoO_x-ZIF.**

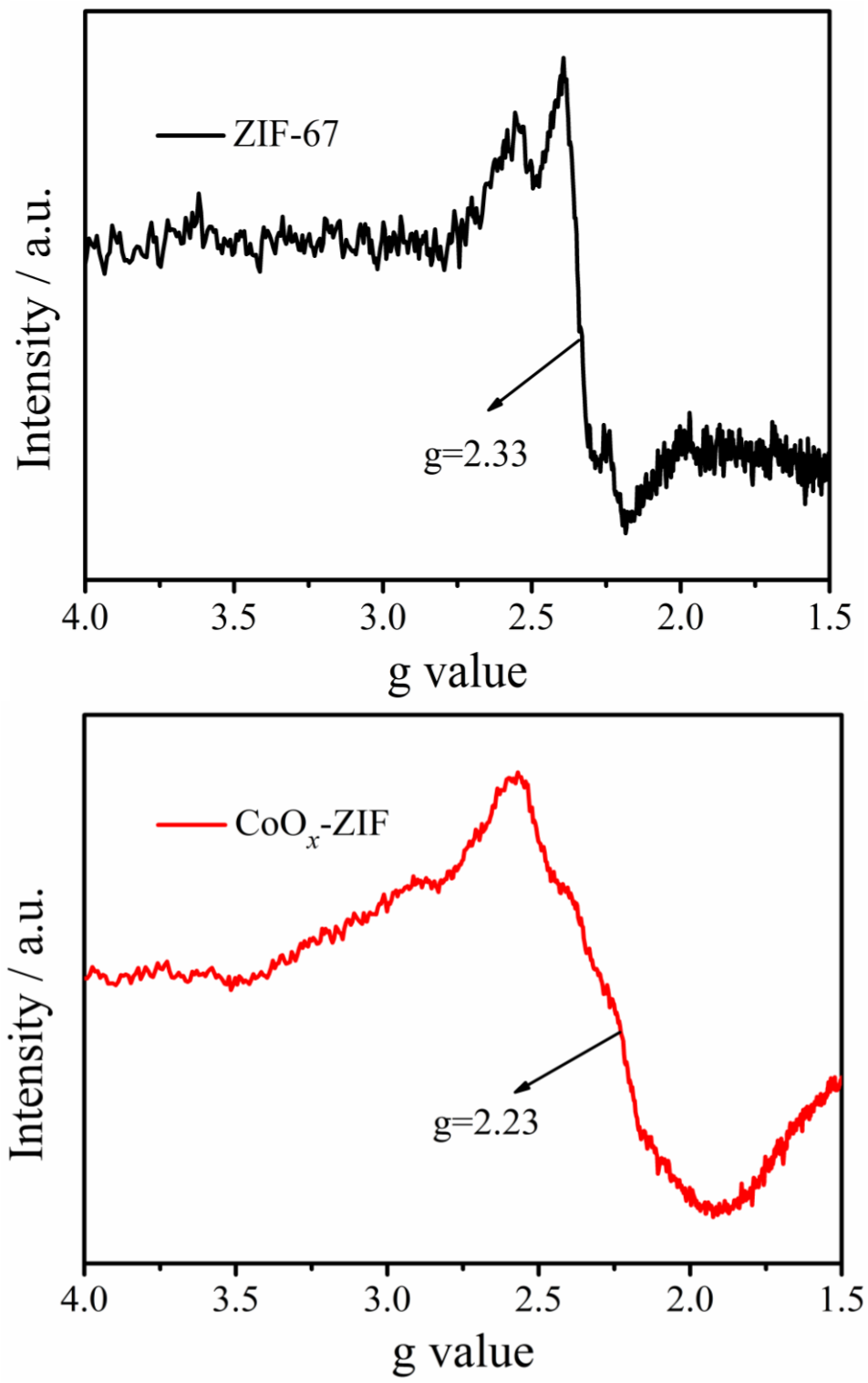

Figure S10. **EPR spectra of ZIF-67 and CoO_x-ZIF.**

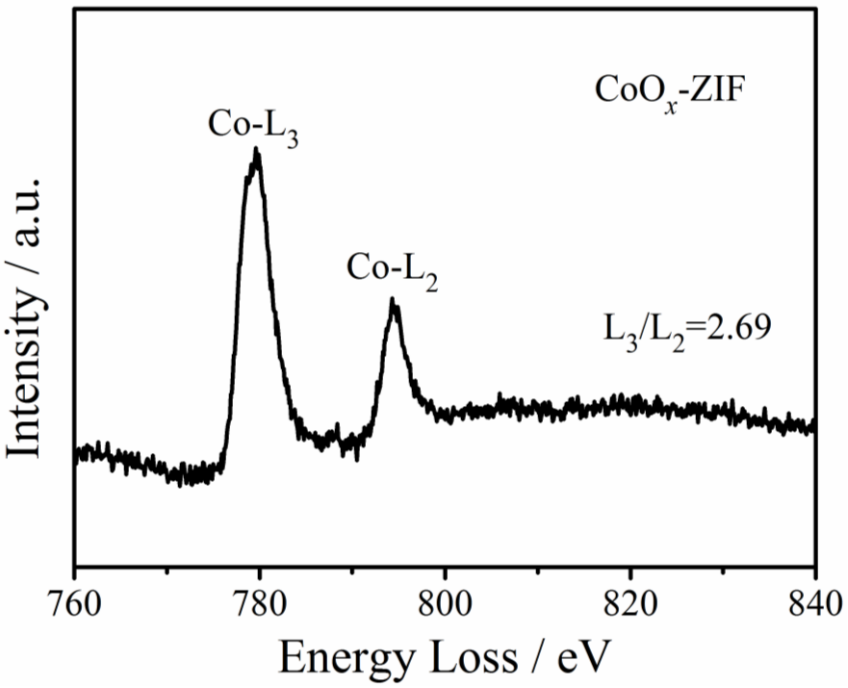

Figure S11. **EELS spectra of CoO_x-ZIF.**

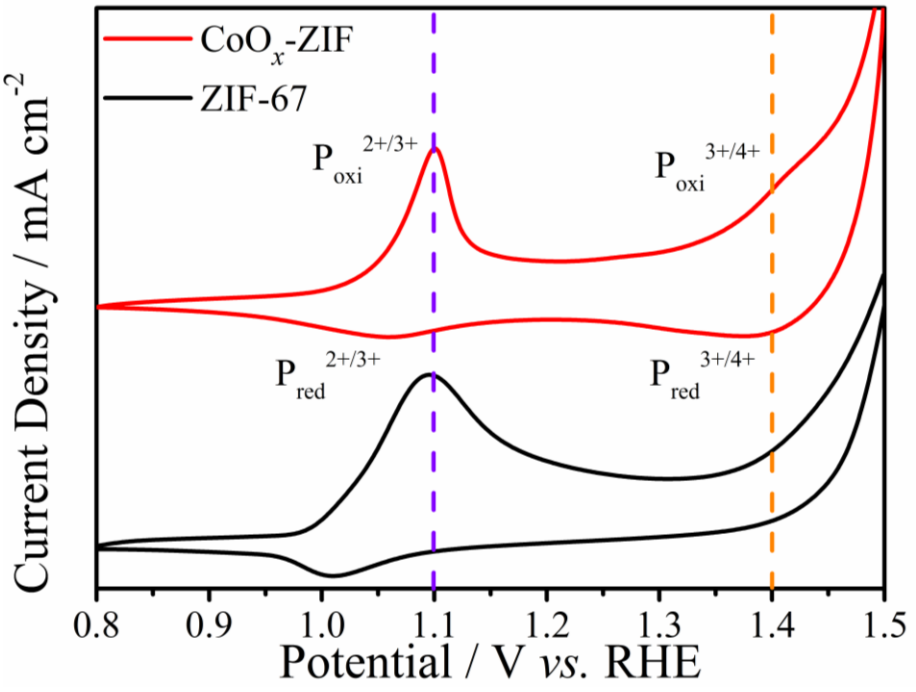
CoO$_x$-ZIF
ZIF-67
P$_{oxi}^{2+/3+}$
P$_{oxi}^{3+/4+}$
P$_{red}^{2+/3+}$
P$_{red}^{3+/4+}$
Current Density / mA cm^{-2}
0.8
0.9
1.0
1.1
1.2
1.3
1.4
1.5
Potential / V *vs.* RHE

Figure S12. **CVs curves of CoO_x-ZIF, pristine ZIF-67 in the Co redox region. (each curve is normalized to have a similar redox peak height)**

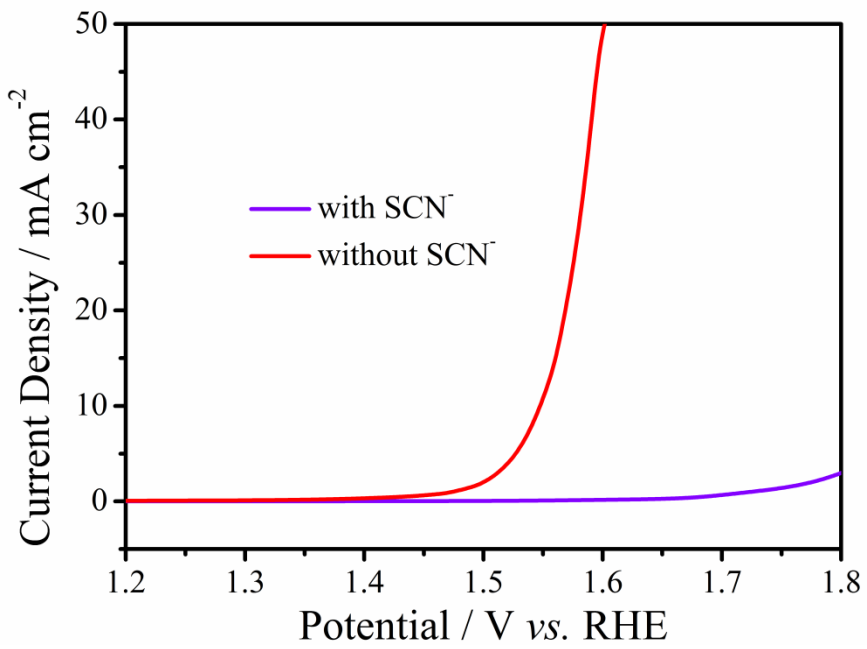

Figure S13. **LSV curves of CoO_x-ZIF in 1 M KOH solution at 1600 rpm with or without 0.1 M SCN^-.**

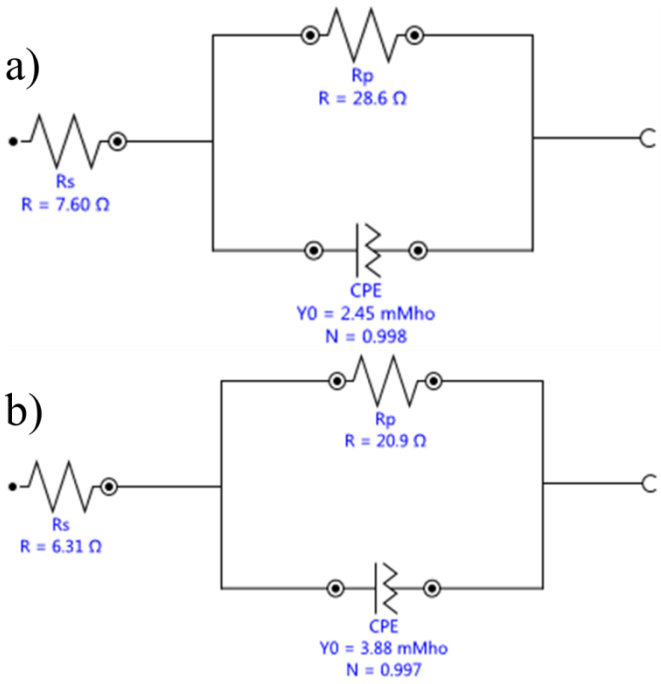

Figure S14. **Electrochemical impedance spectroscopy (EIS) fitting results for a) pure ZIF-67 and b) CoO_x-ZIF. Rs: electrolyte resistance, Rp: charge-transfer resistance, CPE: constant-phase element.**

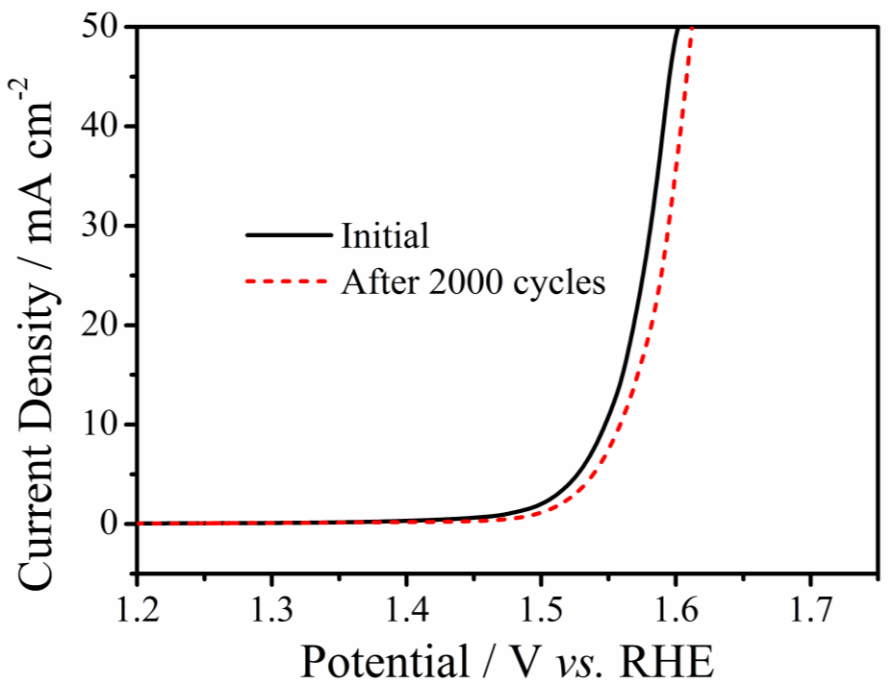

Figure S15. **LSV polarization curves of CoO_x-ZIF before and after cycling for 2000 cycles.**

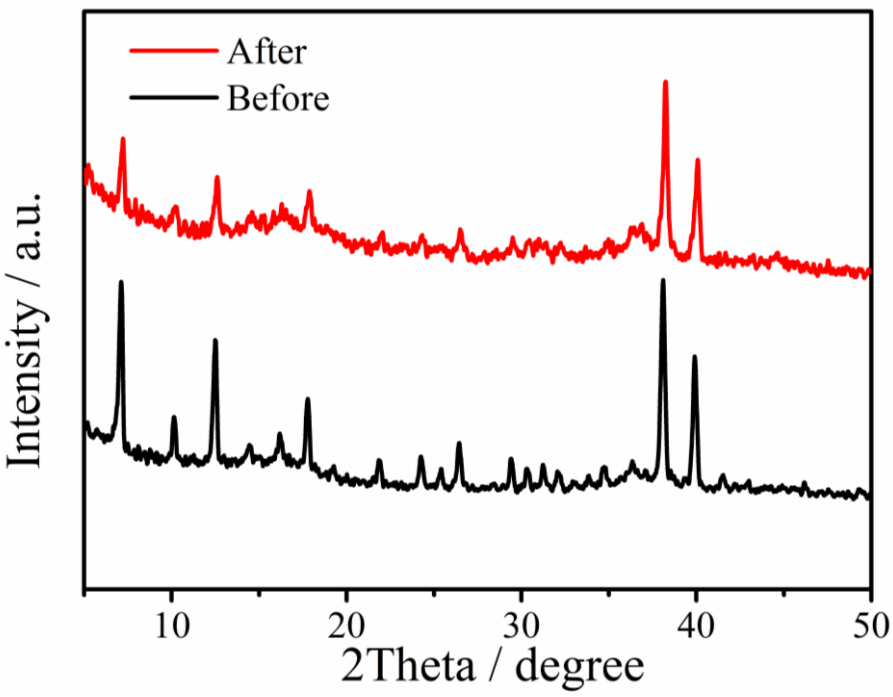

Figure S16. **XRD patterns of CoO_x-ZIF on Ti sheet before and after cycling for 2000 cycles.**

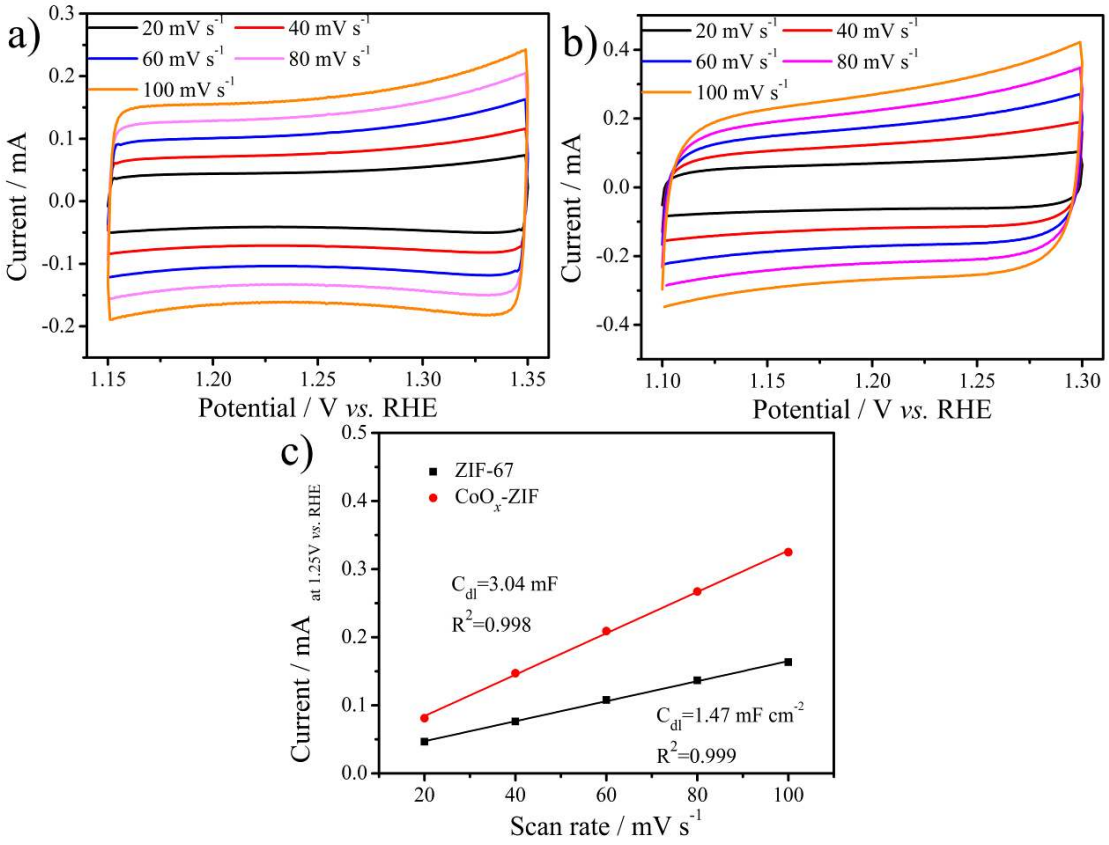

Figure S17. **ESCA tests of pure ZIF-67 and CoO_x-ZIF towards OER in 1 M KOH. a) CV curves of ZIF-67 and b) CoOx-ZIF with different scanning rates from 20 to 100 mV s^{-1}; c) Charging current plotted against scanning rates at -1.25 V *vs*. RHE.**

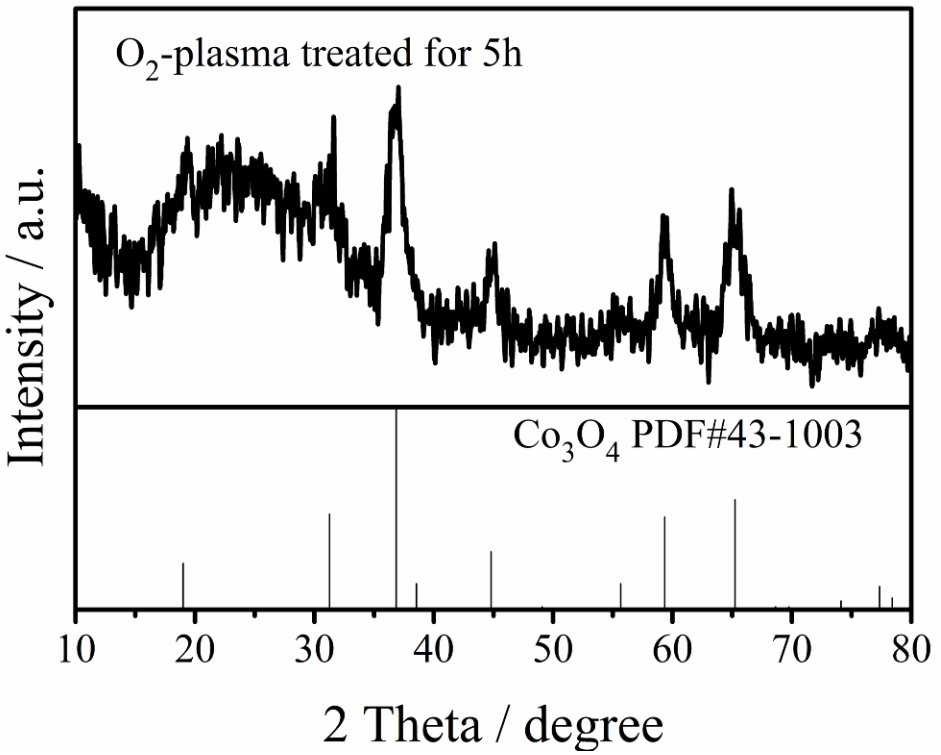

Figure S18. **XRD pattern of the O_2-Plasma treated ZIF-67 for 5h.**

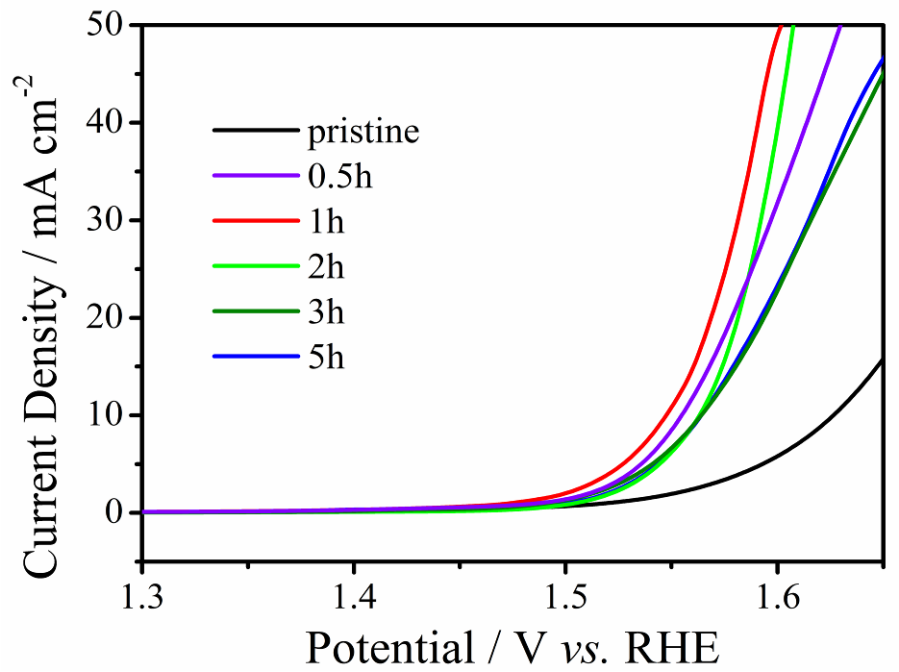

Figure S19. **LSV polarization curves of pristine ZIF-67 and O_2-Plasma treated for different times.**

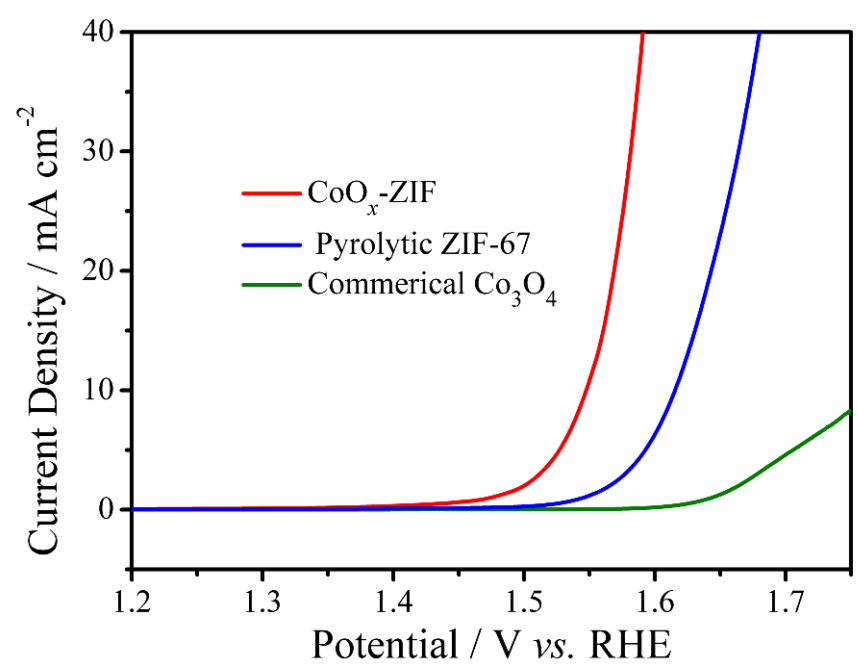

Figure S20. **LSV polarization curves of CoO_x-ZIF, pyrolyzed ZIF-67 and commercial Co_3O_4.**

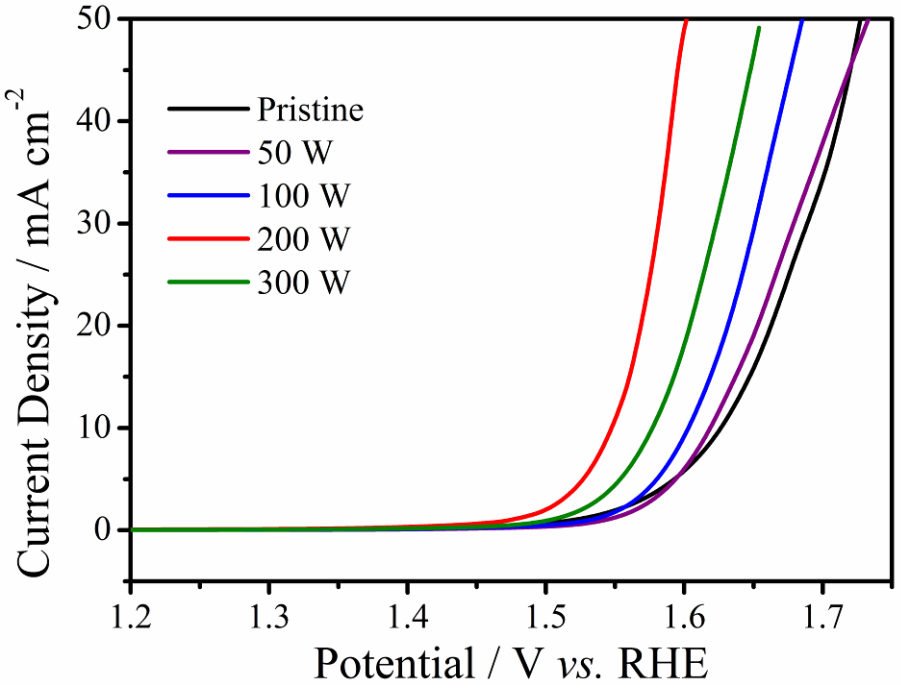

Figure S21. **LSV polarizationcurves of O_2-plasma treated ZIF-67 with different RF power.**

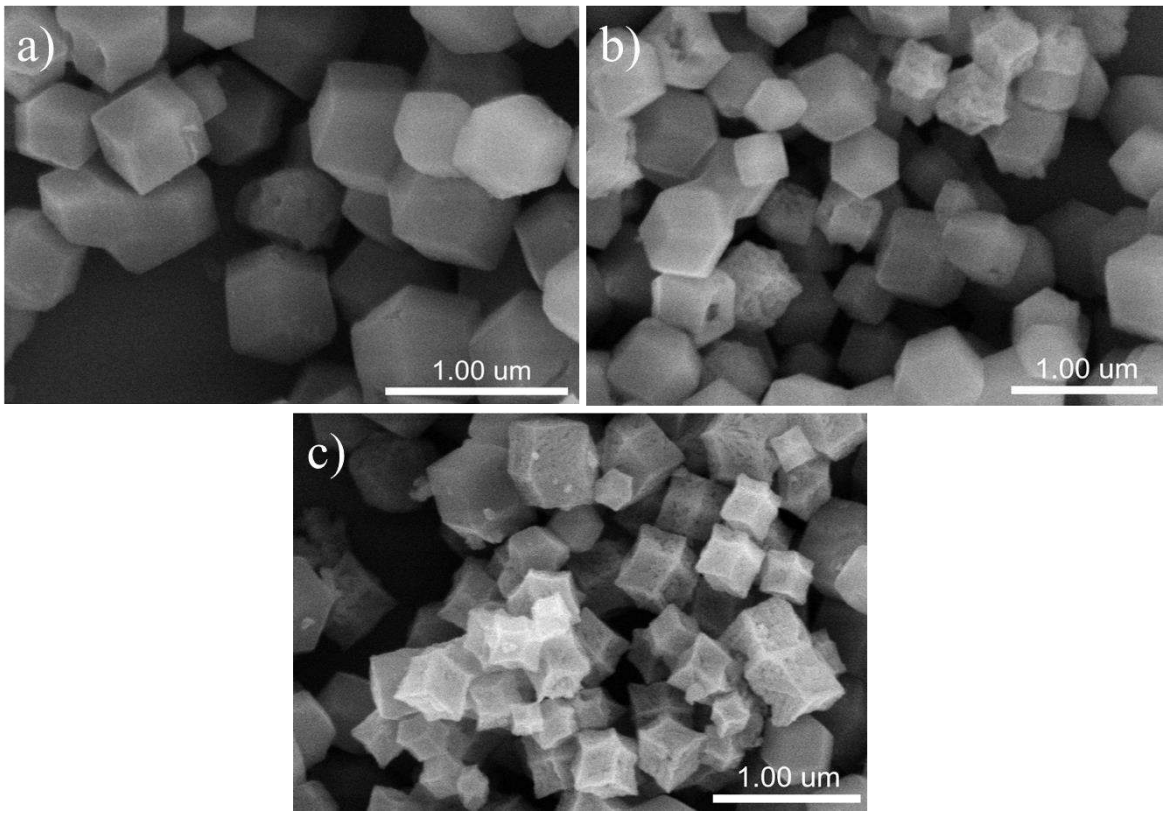
a)
1.00 um
b)
1.00 um
c)
1.00 um

Figure S22. **SEM images of O_2-plasma treated ZIF-67 with different RF power: a) 50 W; b) 100 W; c) 300 W.**

Table S3. Comparison of OER activity of the CoO_x-ZIF with recently reported catalysts.

Catalysts	Preparation temperature (°C)	Potential at j=10 mA cm^{-2} (mV)	Tafel slope (mV dec^{-1})	Electrolyte	Substrate	Ref.
CoO_x-ZIF	Room temperature	1.548	70.3	1M KOH	Glassy carbon	This work
N-CG-CoO	750	1.57	70	1M KOH	Glassy carbon	[1]
Co_3O_4C-NA	500	1.52	70	0.1M KOH	Cu foil	[2]
CoO_x@CN	800	~1.60	N.A.	1M KOH	Glassy carbon	[3]
Co_3O_4 NW	400	1.55	72	1M KOH	Carbon cloth	[4]
$Ni_xCo_{3-x}O_4$ NW	400	1.59	59~64	1M KOH	Ti foam	[5]
Co@Co_3O_4/NC	800	1.64	54.3	0.1M KOH	Glassy carbon	[6]
Co_3O_4@C-MWCNTs	700	1.55	62	1M KOH	Glassy carbon	[7]
Co_9S_8@NOSC-900	900	1.56	68	1M KOH	Nickel foam	[8]
N/Co-doped PCP//NRGO	900	1.66	292	0.1M KOH	Glassy carbon	[9]

[1] Mao S.,Wen Z.,Huang T.,Hou Y., and Chen J., *Energy & Environmental Science,* 2014, **7**: 609-616.
[2] Ma T. Y.,Dai S.,Jaroniec M., and Qiao S. Z., *J. Am. Chem. Soc.,* 2014, **136**: 13925-31.

[3] Jin H.,Wang J.,Su D.,Wei Z.,Pang Z., and Wang Y., *J. Am. Chem. Soc.,* 2017, **137**: 2688.
[4] Chen P.,Xu K.,Fang Z.,Tong Y.,Wu J.,Lu X.,Peng X.,Ding H.,Wu C., and Xie Y., *Angew. Chem.,* 2015, **54**: 14710.
[5] Li Y.,Hasin P., and Wu Y., *Adv. Mater.,* 2010, **22**: 1926.
[6] Aijaz A.,Masa J.,Rösler C.,Xia W.,Weide P.,Botz A. J.,Fischer R. A.,Schuhmann W., and Muhler M., *Angew. Chem.,* 2016, **55**: 4087.
[7] Li X.,Fang Y.,Lin X.,Tian M.,An X.,Fu Y.,Li R.,Jin J., and Ma J., *Journal of Materials Chemistry A,* 2015, **3**: 17392-17402.
[8] Huang S.,Meng Y.,He S.,Goswami A.,Wu Q.,Li J.,Tong S.,Asefa T., and Wu M., *Adv. Funct. Mater.,* 2017, **27**.
[9] Hou Y.,Wen Z.,Cui S.,Ci S.,Mao S., and Chen J., *Adv. Funct. Mater.,* 2015, **25**: 872-882.